Science Translational Medicine

22 NOVEMBER 2017

AAAS

Science Translational Medicine

Targeting STUB1–tissue factor axis normalizes hyperthrombotic uremic phenotype without increasing bleeding risk

Moshe Shashar, Mostafa E. Belghasem, Shinobu Matsuura, Joshua Walker, Sean Richards, Faisal Alousi, Keshab Rijal, Vijaya B. Kolachalama, Mercedes Balcells, Minami Odagi, Kazuo Nagasawa, Joel M. Henderson, Amitabh Gautam, Richard Rushmore, Jean Francis, Daniel Kirchhofer, Kumaran Kolandaivelu, David H. Sherr, Elazer R. Edelman, Katya Ravid and Vipul C. Chitalia

Sci Transl Med **9**, eaam8475.
DOI: 10.1126/scitranslmed.aam8475

Striking a balance for anticoagulation

Patients with chronic kidney disease can present a therapeutic conundrum because they are not only at increased risk of blood vessel thrombosis but also more likely to experience bleeding complications when treated with anticoagulants. Shashar *et al.* examined the mechanism of thrombosis in mouse models of renal disease and found a potential therapeutic target in a protein called STUB1. STUB1 is a ubiquitin ligase that interacts with tissue factor, a vascular wall protein that triggers the coagulation signaling cascade. The authors demonstrated that increase in STUB1 can prevent thrombosis but does not prolong bleeding in mouse models of kidney disease, suggesting that this may be a viable approach to antithrombotic management of patients.

COAGULATION

Targeting STUB1–tissue factor axis normalizes hyperthrombotic uremic phenotype without increasing bleeding risk

Moshe Shashar,[1]* Mostafa E. Belghasem,[2]* Shinobu Matsuura,[3] Joshua Walker,[1] Sean Richards,[1] Faisal Alousi,[1] Keshab Rijal,[1] Vijaya B. Kolachalama,[3] Mercedes Balcells,[4,5] Minami Odagi,[6] Kazuo Nagasawa,[6] Joel M. Henderson,[2] Amitabh Gautam,[7] Richard Rushmore,[8] Jean Francis,[1] Daniel Kirchhofer,[9] Kumaran Kolandaivelu,[4,10] David H. Sherr,[11] Elazer R. Edelman,[4,10] Katya Ravid,[3] Vipul C. Chitalia[1,2,3†]

Chronic kidney disease (CKD/uremia) remains vexing because it increases the risk of atherothrombosis and is also associated with bleeding complications on standard antithrombotic/antiplatelet therapies. Although the associations of indolic uremic solutes and vascular wall proteins [such as tissue factor (TF) and aryl hydrocarbon receptor (AHR)] are being defined, the specific mechanisms that drive the thrombotic and bleeding risks are not fully understood. We now present an indolic solute–specific animal model, which focuses on solute-protein interactions and shows that indolic solutes mediate the hyperthrombotic phenotype across all CKD stages in an AHR- and TF-dependent manner. We further demonstrate that AHR regulates TF through STIP1 homology and U-box–containing protein 1 (STUB1). As a ubiquitin ligase, STUB1 dynamically interacts with and degrades TF through ubiquitination in the uremic milieu. TF regulation by STUB1 is supported in humans by an inverse relationship of STUB1 and TF expression and reduced STUB1-TF interaction in uremic vessels. Genetic or pharmacological manipulation of STUB1 in vascular smooth muscle cells inhibited thrombosis in flow loops. STUB1 perturbations reverted the uremic hyperthrombotic phenotype without prolonging the bleeding time, in contrast to heparin, the standard-of-care antithrombotic in CKD patients. Our work refines the thrombosis axis (STUB1 is a mediator of indolic solute–AHR-TF axis) and expands the understanding of the interconnected relationships driving the fragile thrombotic state in CKD. It also establishes a means of minimizing the uremic hyperthrombotic phenotype without altering the hemostatic balance, a long-sought-after combination in CKD patients.

INTRODUCTION

Chronic kidney disease (CKD/uremia) imposes a strong and independent risk for both venous and arterial thrombosis in addition to conventional risk factors (*1*–*4*). CKD-associated thrombotic propensities introduce variability, which is not accounted for in the clinical thrombosis risk assessment nor targeted by contemporary antithrombotic/antiplatelet therapies. This variability contributes to their suboptimal efficacy in several clinical postinjury arterial thrombosis scenarios such as angioplasty, stenting, or vascular surgeries in CKD patients (*2*, *5*–*7*).

Vessel wall factors are critical triggers for the postvascular injury thrombosis, where denuded endothelium and exposed vascular smooth muscle cells (vSMCs) create a highly reactive vascular bed. Tissue factor (TF), a potent procoagulant protein and the driver of postinjury thrombosis models, is two- to threefold higher in vSMCs in the uremic milieu and enhances thrombosis (*8*, *9*). Retention of a distinct set of metabolites characterizes the state of uremia, including indolic solutes such as indoxyl sulfate (IS), which are particularly vasculotoxic (*10*). They enhance TF expression by activating the aryl hydrocarbon receptor (AHR) pathway, and AHR antagonists destabilize and down-regulate TF in the uremic milieu (*11*). Although IS and AHR are emerging regulators of TF, their contribution to the thrombotic uremic milieu and the mechanism in CKD warrant further elucidation, because better understanding will help design improved approaches to minimize CKD-specific thrombosis risk.

It is also imperative to weigh the antithrombotic benefit of the approach to bleeding risk in CKD patients, because uremia is a state of bleeding diathesis (*12*). This risk is further exacerbated by current antithrombotics (*13*), which target the hemostatic defenses in the blood. Even newer antithrombotics that are deemed safer, although not tested specifically in the uremic milieu, may function suboptimally in CKD, because none target CKD-specific risk factors (*14*) and may paradoxically enhance thrombosis due to altered baseline platelet reactivity in CKD (*15*). Targeting CKD-associated thrombotic factors is likely to lower the thrombosis risk to non-CKD range and may create a milieu more conducive to current antithrombotics/antiplatelet agents. Such a strategy is also likely to be safer, because it will leave the hemostatic defense in blood intact.

We demonstrate IS as an AHR-dependent mediator of the hyperthrombotic uremic milieu all across the CKD spectrum and show that

[1]Renal Section, Department of Medicine, Boston University School of Medicine, Boston, MA 02118, USA. [2]Department of Pathology and Laboratory Medicine, Boston University School of Medicine, Boston, MA 02118, USA. [3]Department of Medicine and Whitaker Cardiovascular Institute, Boston University School of Medicine, Boston, MA 02118, USA. [4]Institute of Medical Engineering and Science, Massachusetts Institute of Technology, Cambridge, MA 02139, USA. [5]Biological Engineering Department, Institut Químic de Sarrià, Universitat Ramon Llull, Barcelona 08017, Spain. [6]Tokyo University of Agriculture and Technology, 2-24-16 Naka-cho, Koganei, Tokyo 184-8588, Japan. [7]Department of Surgery, Boston University School of Medicine, Boston, MA 02118, USA. [8]Department of Anatomy and Neurobiology, Boston University School of Medicine, Boston, MA 02118, USA. [9]Department of Early Discovery and Biochemistry, Genentech Inc., South San Francisco, CA 94080, USA. [10]Cardiovascular Division, Brigham and Women's Hospital, Harvard Medical School, Boston, MA 02115, USA. [11]Department of Environmental Health, School of Public Health, Boston University School of Medicine, Boston, MA 02118, USA.
*These authors contributed equally to this work.
†Corresponding author. Email: vichital@bu.edu

AHR regulates TF through the STIP1 homology and U-box–containing protein 1 (STUB1), a ubiquitin ligase. We also demonstrate that the perturbation of STUB1 reverts the CKD-associated thrombosis risk to nonuremic range without altering hemostasis.

RESULTS

IS mediates a hyperthrombotic uremic phenotype in an AHR- and TF-dependent manner across the spectrum of CKD

To examine the mediators of the hyperthrombotic uremic milieu in vivo, we considered different animal models of CKD (*16*). The renal damage inflicted in all of these CKD models results in retention of a whole host of uremic solutes and precludes probing of a thrombosis axis initiated by a specific uremic solute. Furthermore, contrary to human CKD, 5/6 nephrectomy model of CKD failed to show enhanced thrombosis (*17*). Therefore, we set out to create a solute-specific animal model that faithfully recapitulates the hyperthrombotic uremic phenotype. Because IS increases TF (*8*, *11*, *18*), we hypothesized that IS will enhance thrombosis. Toward that end, we developed an animal protocol to increase the amount of IS similar to that seen in patients with advanced CKD [CKD stage 5/end-stage renal disease (ESRD)] by administering IS and inhibiting its excretion through the organic anion transporter (OAT) channel using probenecid (*19*). Of the different tested protocols, a combination of IS (4 mg/ml) in water given ad libitum and probenecid (150 mg/kg, intraperitoneally) twice a day increased IS concentrations beyond those of ESRD patients and was selected for further experiments (Fig. 1A and fig. S1A). Probenecid used in this model inhibited renal excretion of IS. Given the ubiquitous expression of OAT channels (*19*), probenecid may also compromise the entry of IS into the cells. However, we posited that high blood concentration of IS resulting from the above protocol will ensure sufficient intracellular IS concentrations to activate AHR, even in the presence of probenecid. Toward that end, we examined AHR activation in the vessels of mice that received IS + probenecid, using an AHR decay assay (fig. S1, B and C). The assay is based on the observation that AHR activation with an agonist ligand such as IS eventually results in the degradation of AHR protein (*11*). Thus, AHR expression is likely to be lower in the vessels of animals exposed to IS + probenecid if intracellular concentration of IS rises in the presence of probenecid. The aortae of IS + probenecid mice harvested at different time points showed a significant (*P* values ranging from 0.003 to <0.001) and persistent reduction in AHR throughout the duration of exposure, as compared to probenecid controls (fig. S1, B and C). In addition, a striking increase in TF was observed in their aortae (fig. S1D). Together, these data show that the increase in IS concentrations in the vessel walls is sufficient to activate AHR-TF signaling in mice exposed to IS + probenecid.

After confirming the activation of the AHR-TF axis in the vessel walls of these animals, we examined thrombogenicity in the carotid artery with the $FeCl_3$ postinjury thrombosis model (*20*). The primary end point was time to occlusion (TtO), which corresponds to the carotid blood flow between 0 and 0.2 ml/min (Fig. 1B and fig. S1E) (*20*) and was validated by the presence of an occlusive thrombus at the site of injury (Fig. 1C). From a range of $FeCl_3$ concentrations tested, 10% $FeCl_3$ resulted in the smallest SD and was adopted for subsequent experiments (fig. S1F).

Under these optimized conditions, IS significantly (P =0.001) reduced TtO (Fig. 1D), which was reversed with the AHR antagonist CH223191 (P = 0.005) (*11*) or previous infusion of a prevalidated anti-mouse anti-TF neutralizing antibody (P = 0.021; Fig. 1E) (*21*). To further confirm the thrombogenicity of IS, we induced thrombosis by photoactivated rose bengal dye, which produces singlet oxygen to damage endothelial cell membranes (*22*). Consistent with the $FeCl_3$ model, IS-treated animals showed a significant reduction in TtO after photochemical injury (P = 0.017; Fig. 1F). Whereas these two models examined the prothrombotic properties of IS at concentrations corresponding to advanced CKD, we next probed its role in early stages of CKD, because patients with mild CKD are also predisposed to enhanced thrombosis (*11*, *23*). IS concentrations corresponding to the different stages of CKD were achieved in the blood of animals by titrating the IS concentration in water. Resultant blood concentrations of IS were determined and correlated to the TtO. The data showed a significant inverse correlation between TtO and IS concentrations corresponding to all CKD stages (P < 0.0001; Fig. 1G). Overall, the above results support IS as an AHR- and TF-dependent mediator of the hyperthrombotic uremic milieu across the entire CKD spectrum.

AHR regulates TF through STUB1, a ubiquitin ligase for TF

Because the above data implicated IS as a strong contributor to the hyperthrombotic uremic phenotype, we further probed the mechanism of IS-induced changes in AHR/TF, which promote thrombogenicity. We found that STUB1, a ubiquitin ligase and an AHR interactor, mediated the effect of IS/AHR on TF (*24*). *STUB1* silencing in primary human aortic vSMCs and human umbilical vein endothelial cells (thrombosis-relevant cell types) showed significantly increased TF expression (P = 0.001) (Fig. 2A and fig. S2A) and TF activity in both uremic and nonuremic milieu (Fig. 2B). In line with STUB1's ubiquitin ligase function (*24*, *25*), *STUB1*-silenced vSMCs showed a significantly (P < 0.001) prolonged TF half-life under the uremic condition, from 3.25 hours to more than 8 hours (Fig. 2, C and D), and reduced ubiquitination (fig. S2B). CB7993113, a competitive AHR antagonist (*11*), reduced TF expression by 80% (from 1.0 to 0.21), whereas it was only reduced by 30% (from 2.7 to 1.98) with a concomitant *STUB1* silencing (Fig. 2E). *STUB1* silencing also abrogated CB7993113-mediated TF ubiquitination in the uremic milieu (Fig. 2F). Consistent with the above results, mesenchymal embryonic fibroblasts (MEFs) from STUB1 knockout (KO) animals (*25*) showed a significant increase in TF expression (P = 0.001) and activity (P = 0.003) and reduced TF ubiquitination (fig. S2, C to E). Ubiquitin ligase–dependent STUB1 regulation of TF was further demonstrated using a ubiquitin ligase–deficient H260Q STUB1 mutant (*25*). Compared to STUB1 wild-type (WT), the H260Q mutant showed little effect on TF ubiquitination (fig. S2F). The above results suggest that STUB1 mediates TF ubiquitination and that AHR antagonist augments TF down-regulation through STUB1.

Uremia-dependent STUB1-TF interaction is dynamic

Ubiquitination is a nonlinear process consisting of a complex interdigitated set of regulated steps, which include ubiquitin activation, conjugation, and transfer of the ubiquitin moiety to the target molecule (*26*). This process requires a precise and dynamic interaction between a ligase and its putative target. Reciprocal immunoprecipitation assays in vSMCs demonstrated that anti-TF antibodies coimmunoprecipitated STUB1 and vice versa (fig. S3A). An in vitro binding assay demonstrated a direct binding of recombinant STUB1 to purified human TF protein (Fig. 3A). Immunofluorescence studies showed colocalization of STUB1 and TF predominantly in the cytosol of vSMCs in normal human artery and cultured vSMCs with Pearson's correlation coefficients of 0.50 and 0.82, respectively (fig. S3, B to F) (*27*). Although these data indicated a constitutive interaction between STUB1 and TF, the STUB1-TF interaction was dynamic and dependent on the uremic status.

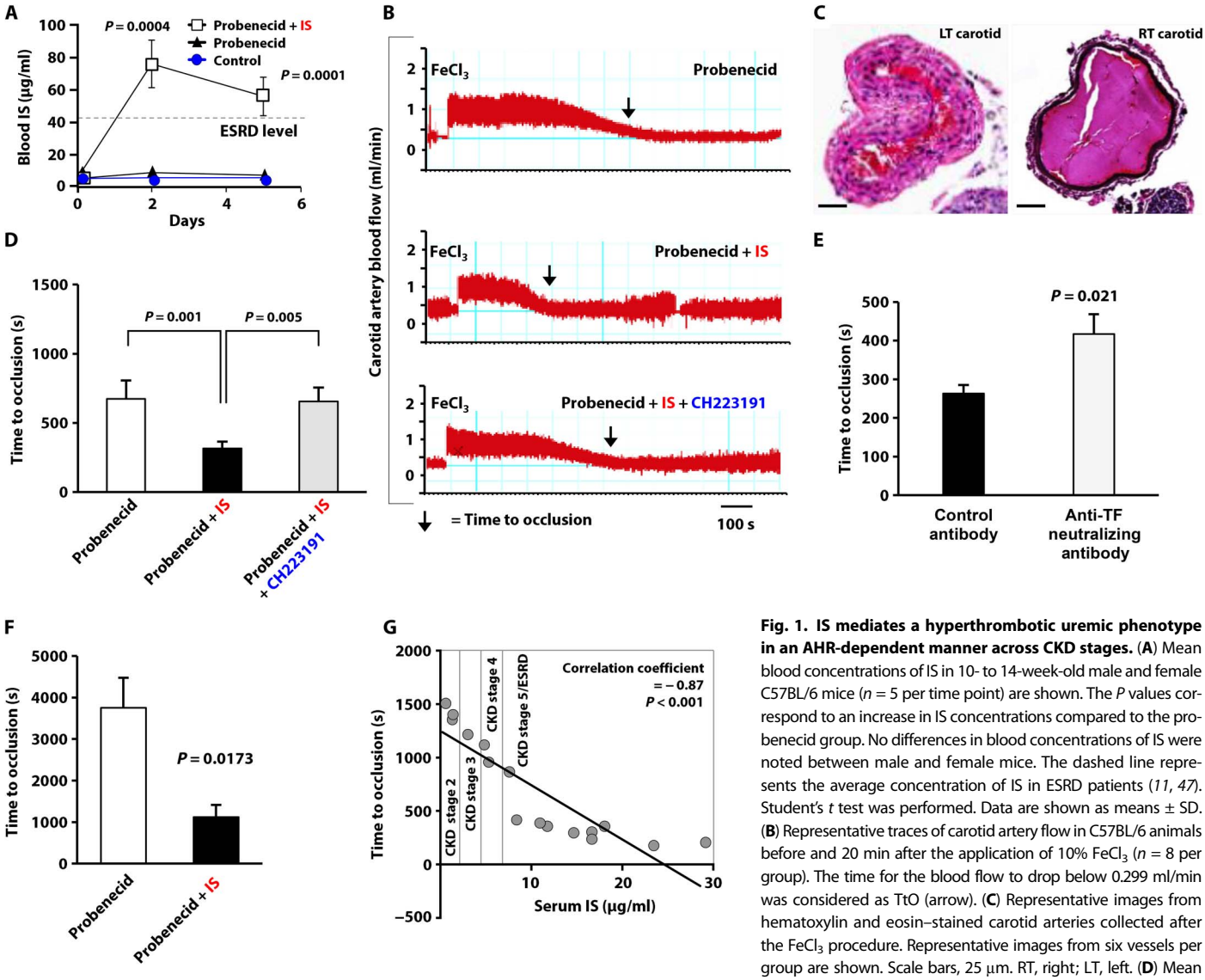

Fig. 1. IS mediates a hyperthrombotic uremic phenotype in an AHR-dependent manner across CKD stages. (**A**) Mean blood concentrations of IS in 10- to 14-week-old male and female C57BL/6 mice ($n = 5$ per time point) are shown. The P values correspond to an increase in IS concentrations compared to the probenecid group. No differences in blood concentrations of IS were noted between male and female mice. The dashed line represents the average concentration of IS in ESRD patients (*11*, *47*). Student's t test was performed. Data are shown as means ± SD. (**B**) Representative traces of carotid artery flow in C57BL/6 animals before and 20 min after the application of 10% $FeCl_3$ ($n = 8$ per group). The time for the blood flow to drop below 0.299 ml/min was considered as TtO (arrow). (**C**) Representative images from hematoxylin and eosin–stained carotid arteries collected after the $FeCl_3$ procedure. Representative images from six vessels per group are shown. Scale bars, 25 μm. RT, right; LT, left. (**D**) Mean TtO ($n = 8$ per group) after 5 days of exposure to IS and IS + CH223191. Student's t test was performed. Data are shown as means ± SD. (**E**) Mice were exposed to probenecid + IS for 5 days and then subjected to the $FeCl_3$ thrombosis assay. Thirty minutes before the assay, control antibody or rat anti-mouse TF neutralizing antibody was administered. Mean TtO ($n = 6$ per group) is shown. Data are shown as means ± SEM. (**F**) Mean TtO in the photochemical thrombosis model in probenecid and probenecid + IS mice ($n = 6$ per group). Student's t test was performed. Data are shown as means ± SEM. (**G**) Relationship between TtO and different concentrations of IS in 16 animals. IS concentrations from different stages of human CKD are shown (*3*, *11*). A Pearson correlation analysis was performed.

STUB1-TF interaction reduced substantially with IS (Fig. 3B) and increased within 20 min of AHR antagonist treatment. This rapidity of increased STUB1-TF interaction induced by AHR antagonist is consistent with the previously observed restoration of TF ubiquitination and shortened TF half-life with AHR antagonist (*11*). Together, the above data suggest that uremia reduces STUB1-TF interaction and stabilizes TF and that AHR antagonists rapidly restore this interaction.

Furthermore, the site of interaction of STUB1 and TF corroborated the above binding pattern. Because STUB1 is a cytosolic protein (*28*) and TF has a cytosolic C terminus (fig. S3G) (*29*), STUB1 is likely to target the C-terminal tail of TF. Domain mapping was performed by comparing the WT TF (TF-WT) with a TF truncation lacking its C terminus (TFdelC). STUB1 interacted with TF-WT but not TFdelC (Fig. 3C) and down-regulated it (but not TFdelC) by 70% (time, 0; Fig. 3, D and E). STUB1 also significantly shortened the half-life of TF-WT ($P = 0.006$) (fig. S3H) and increased its ubiquitination (Fig. 3F). STUB1 did not destabilize (Fig. 3E and fig. S3I) or ubiquitinate TFdelC (Fig. 3F), indicating that STUB1 targets the C-terminal tail of TF for ubiquitination and degradation.

STUB1-TF relationship in human tissue is uremia-dependent

Dynamic interaction with and regulation of TF by STUB1 were further substantiated in human vascular tissue using immunofluorescence studies of explanted arteriovenous fistulae (AVFs), unique vascular conduits required in patients with advanced CKD, which are frequently prone to thrombosis (*30*). The vSMCs within the walls of AVF explants

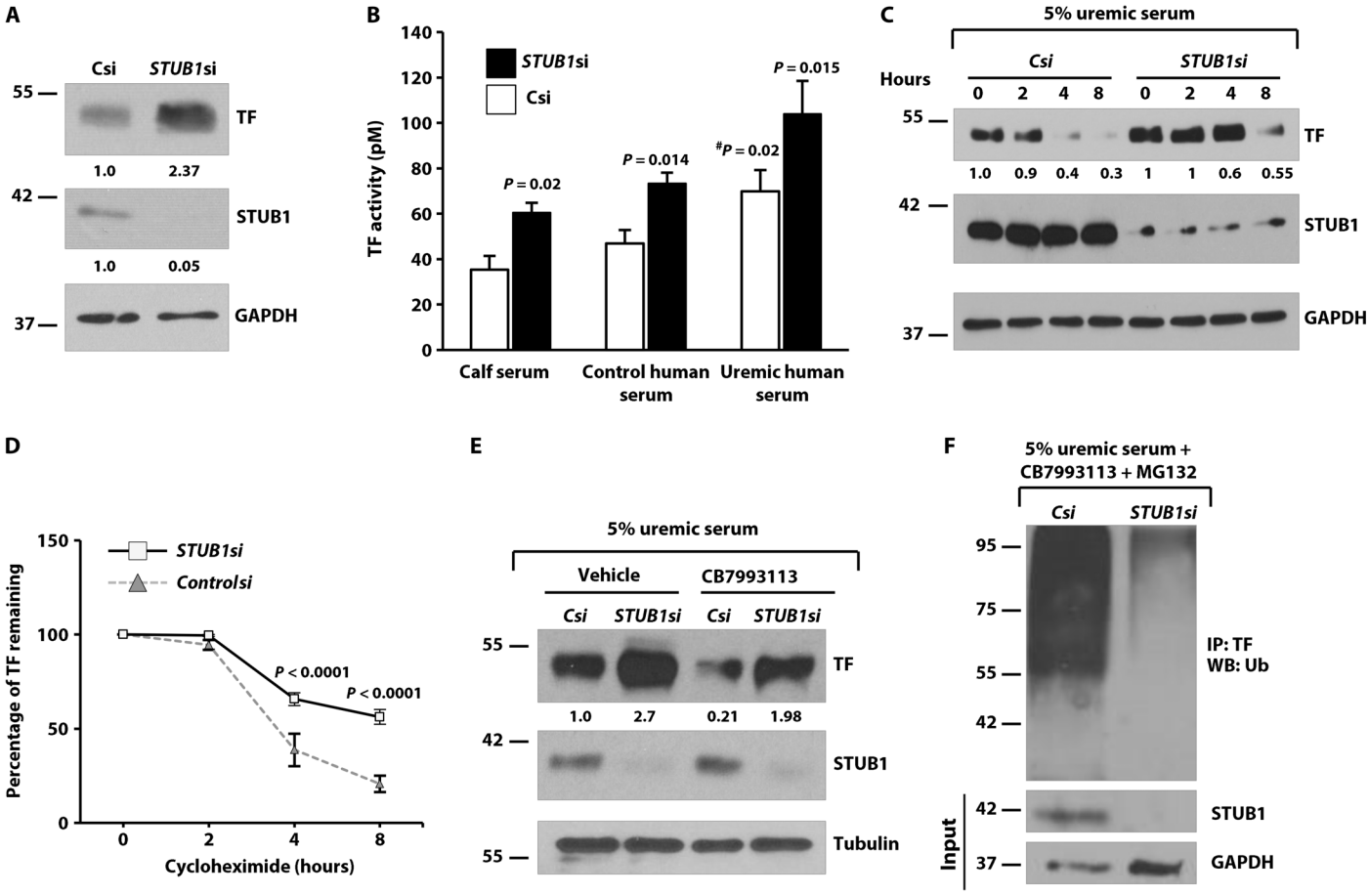

Fig. 2. STUB1 destabilizes and ubiquitinates TF and mediates TF regulation by AHR. (**A**) Lysates from primary human aortic vSMCs transfected with control (Csi) or *STUB1* silencing oligonucleotides (*STUB1si*) were probed for TF and normalized to glyceraldehyde-3-phosphate dehydrogenase (GAPDH) using ImageJ. Equal amounts of lysates were separately probed for STUB1 to avoid stripping of blots for the proteins with molecular weights in close range, a strategy also applied to other figures. Expression of TF and STUB1 normalized to the loading control is shown below this and subsequent Western blots. A representative figure from four independent experiments is shown. (**B**) vSMCs pretransfected with Csi and *STUB1si* were stimulated with 5% of the indicated type of serum for 24 hours. A mean TF activity of two independent experiments performed in duplicates is shown. Student's *t* test was performed. Number sign (#) corresponds to TF activity in Csi vSMCs treated with uremic compared to control serum. Other *P* values correspond to *STUB1*-silenced compared to Csi cells. Data are shown as means ± SD. (**C**) vSMCs pretransfected with *Csi* and *STUB1si* grown in 5% uremic serum for 24 hours and then treated with cycloheximide (80 μM) to inhibit protein translation for the indicated time. Equal amounts of lysates were probed separately to confirm *STUB1* silencing. TF expression normalized to the loading control is depicted below the blot. A representative figure from four independent experiments is shown. (**D**) Densitometry of normalized TF expression is represented as the percentage of TF at time 0. The time to reach 50% of initial TF was considered as the half-life of TF. An average of four experiments is shown. Data are shown as means ± SD. (**E**) vSMCs pretransfected with *Csi* and *STUB1si* were treated with 5% uremic serum with or without the AHR antagonist CB7993113 (20 μM) or vehicle for 24 hours. A representative of two independent experiments performed in duplicate is shown. (**F**) vSMCs pretransfected with *Csi* and *STUB1si* were treated with 5% uremic serum + 20 μM CB7993113 (12 hours) and 10 μM MG132 (4 hours) before harvest. The lysates immunoprecipitated with anti-TF antibody were probed with anti–ubiquitin (Ub) antibody. Five percent of lysates are shown as inputs. A representative of three independent experiments is shown. IP, immunoprecipitation; WB, Western blotting.

expressed both STUB1 and TF (Fig. 3G). On the basis of the above data (Fig. 2, A, C, and E), we posited an inverse relationship between STUB1 and TF in the uremic milieu. However, the precise demonstration of a relationship between proteins requires their quantification, which is challenging in heterogeneous human tissues using conventional methods (*31*). Therefore, we developed an object-level intensity estimation algorithm to quantify TF and STUB1 expressions. The results showed a strong inverse correlation between TF and STUB1 expression in the vSMCs in the walls of AVFs (Fig. 3, H and I, and table S1). We further posited that reduced STUB1-TF interaction in vSMCs induced by IS (Fig. 3B) is likely to reduce STUB1-TF colocalization in the uremic vessel wall. To this end, we compared the STUB1-TF colocalization in human AVF (uremic vessel) and vessels from non-CKD patients (nonuremic control) using a customized colocalization algorithm with pixel-level analysis (table S1). The results showed an almost 50% reduction in the colocalization of STUB1-TF in uremic compared to nonuremic human vessels (Fig. 3, J and K). Together, these results indicate STUB1's direct and dynamic interaction with and regulation of TF.

STUB1 modulation regulates postinterventional thrombosis

TF from exposed vSMCs is a critical trigger of postinjury thrombosis, especially in the uremic milieu (*8*, *9*). We examined the effect of STUB1 on thrombosis using the flow-loop system (*32*), a validated model of postinterventional thrombosis (Fig. 4, A and B). It specifically examines

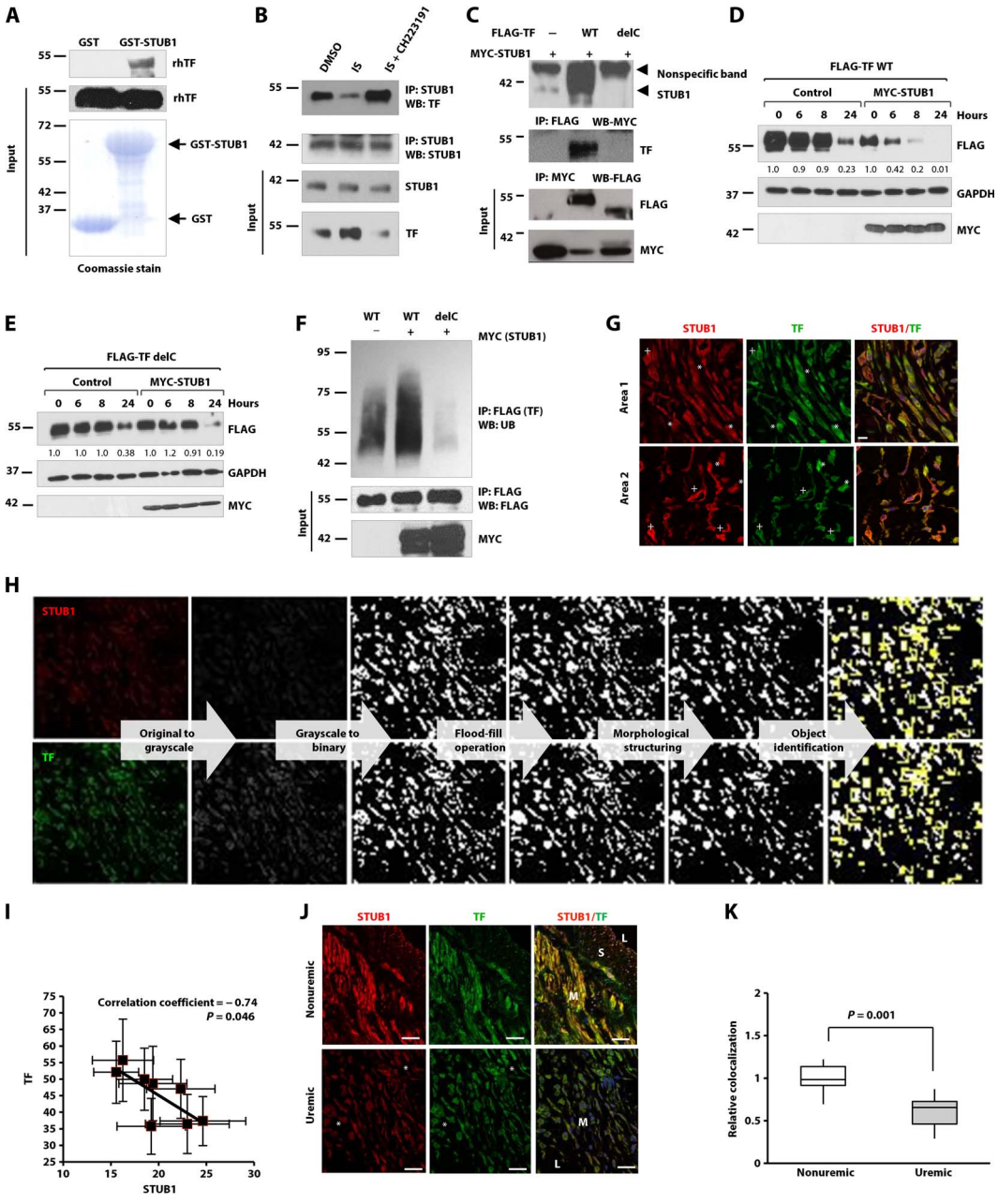

Fig. 3. A dynamic STUB1-TF interaction depends on the uremic status. (**A**) Recombinant GST-tagged STUB1 protein was immobilized on glutathione *S*-transferase (GST) beads and treated with lipidated human recombinant TF (rhTF) protein for 4 hours. Eluents were probed for bound TF. Five percent of recombinant GST-tagged STUB1 stained with Coomassie and recombinant TF are shown as inputs. Representative immunoblots from four independent experiments are shown. (**B**) vSMCs were pretreated with 10 μM IS (24 hours) and 20 μM CH223191 (20 min) followed by immunoprecipitation using anti-STUB1 antibody, and the eluents were probed for TF. The stripped blot was reprobed for STUB1. Five percent of cell lysates are shown as inputs. Representative blots from three independent experiments are shown. DMSO, dimethyl sulfoxide. (**C**) Human embryonic kidney (HEK) 293T cells stably expressing FLAG-tagged WT TF (TF-WT) or TF C-terminal truncation (TFdelC) were transfected with myelocytomatosis (MYC)–tagged STUB1. Cell lysates were immunoprecipitated with FLAG or MYC antibodies, and coimmunoprecipitated proteins were detected using MYC and FLAG antibodies. Five percent of lysates were probed as inputs. A representative of two independent experiments done in duplicates is shown. (**D**) HEK293T cells coexpressing FLAG-tagged WT TF and empty vector (control) or MYC-tagged STUB1 plasmids were treated with cycloheximide for the indicated amount of time. The TF bands were normalized to GAPDH. Equal amounts of lysates were probed for MYC-tagged STUB1. A representative of three independent experiments is shown. (**E**) HEK293T cells coexpressing FLAG-tagged TFdelC and empty vector (control) or MYC-tagged STUB1 were processed as in (D). A representative from three independent experiments is shown. (**F**) HEK293T cells coexpressing FLAG-tagged WT TF (WT) or TFdelC (delC) along with MYC-tagged STUB1 were treated with 10 μM MG132 for 16 hours. The lysates were immunoprecipitated with anti-TF antibodies and probed for ubiquitin. The stripped blot was reprobed with FLAG. Five percent of the cell lysates are shown as inputs. Representative immunoblots from three independent experiments are shown. (**G**) Confocal images of paraffin-embedded sections of an explanted AVF from a 42-year-old male with stage 5 CKD stained with anti-TF and anti-STUB1 antibodies are shown. In different areas of the same AVF, cells with lower STUB1 and higher TF expression are marked by asterisks (*), and cells showing the opposite pattern are marked by crosses (+). The images shown are representative of eight immunofluorescence images acquired from four CKD/ESRD patients. Scale bar, 100 μm. (**H**) Pipeline of object recognition algorithm developed to correlate cell-level intensity distributions of STUB1 with TF (see Materials and Methods for more details). (**I**) Eight immunofluorescence images from four explanted AVFs from CKD/ESRD patients were analyzed using an object recognition algorithm. The intensities of TF and STUB1 within image objects containing vSMCs (average of 187 cells per image; total, 1501 cells) were quantified and averaged for each image. Data are shown as means ± SD. (**J**) Confocal images of paraffin-embedded sections of an explanted AVF from a 47-year-old CKD patient (uremic) and a popliteal artery from a 53-year-old male with normal renal function (nonuremic) (table S1) stained with anti-TF and anti-STUB1 antibodies. Two representatives from a total of eight uremic and nonuremic images are shown. L, lumen; S, subendothelium; M, medium. Asterisks (*) mark areas of cells with low STUB1 and high TF expression similar to those in (G). Scale bars, 100 μm. (**K**) Confocal images acquired from four explanted AVFs from CKD/ESRD patients and popliteal arteries from patients with normal renal function were analyzed using a pixel-level colocalization algorithm. Percentage colocalization of TF-STUB1 was defined as the fraction of pixels with intensity values greater than image-specific thresholds for STUB1 and TF and was compared between the two groups. Data are shown as means ± SD.

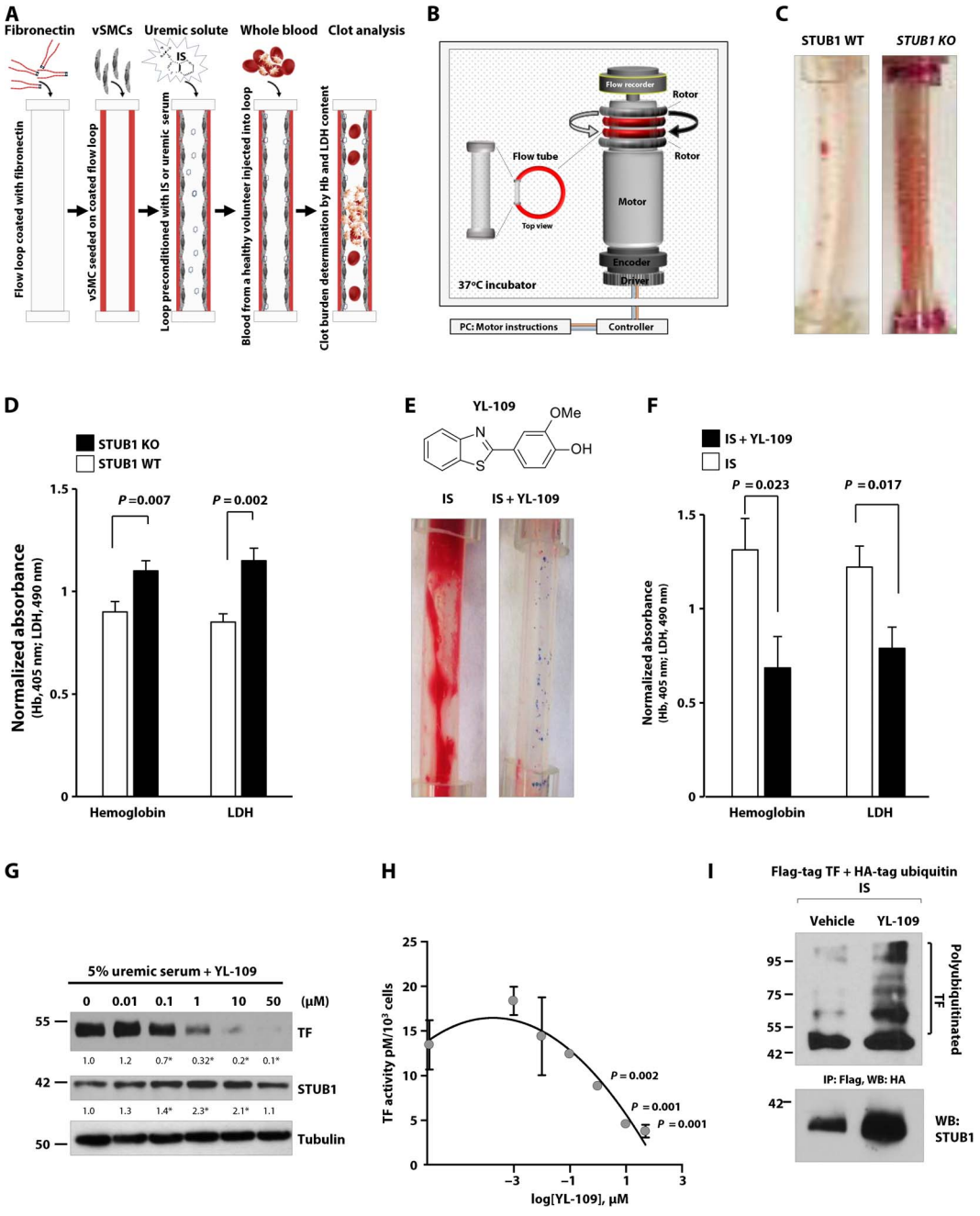

Fig. 4. STUB1 modulation regulates TF activity and thrombosis in a postvascular interventional model. (**A**) Scheme of flow-loop preparation. (**B**) The flow-loop system consists of silastic loops loaded on rotor stages and driven by motors and motion controllers. The tubes injected with the human blood are subjected to coronary-like flow pattern until clotting appears. The wall motion creates bidirectional flows that are measured via onboard, extracorporeal flow probes built into the rotor stages. (**C**) A representative tube from six independent flow loops seeded with STUB1 WT and KO MEFs is shown ($n = 6$ per group). (**D**) Average Hb and LDH from clotted flow loops lined with STUB1 WT and KO MEFs ($n = 6$ per group). Student's t test was performed. Data are shown as means ± SEM. (**E**) Top: Structure of YL-109 (*33*). Bottom: Primary human aortic vSMCs seeded on fibronectin-coated tubes were stimulated with IS (10 μM) with or without YL-109 (25 μM) for 24 hours before loading. A representative tube from six independent flow loops in each group is shown. (**F**) Average Hb and LDH from clotted flow loops pretreated with IS with or without YL-109 ($n = 6$ per group). Data are shown as means ± SEM. (**G**) Lysates of vSMCs pretreated with 5% uremic serum along with the indicated amount of YL-109 for 24 hours were probed for TF and GAPDH. An equal amount of lysates was probed for STUB1. Representative blots from three independent experiments are shown. Student's t test was performed, and asterisk (*) indicates significant changes in TF and STUB1 expressions compared to 5% uremic serum ($P < 0.05$). (**H**) A serum-starved confluent monolayer of vSMCs was treated with 5% uremic serum and YL-109 at different concentrations, and TF activity was measured in picomolar and normalized to 10^3 cells. An average of two independent experiments performed in duplicates is shown. A log dose of YL-109 was plotted against TF activity. Data are shown as means ± SD. (**I**) Primary human aortic vSMCs cotransfected with the FLAG-tag TF and hemagglutinin (HA)–tag ubiquitin plasmids were treated with IS (50 μM) with or without YL-109 (20 μM) for 24 hours and with MG132 (5 μM) for 16 hours before harvest. The lysates were immunoprecipitated using anti-FLAG antibody and probed with anti-HA antibody. Five percent of whole-cell lysates were separately probed for STUB1. A representative blot of three independent experiments is shown.

the blood and vessel wall factor interactions under humanized rheological conditions and can recapitulate thrombosis in the uremic milieu (*8*). The flow loops with STUB1 KO MEFs showed more clot formation (Fig. 4C) and a significantly higher clot burden [increased hemoglobin (Hb), $P = 0.007$; lactate dehydrogenase (LDH), $P = 0.002$; Fig. 4D). Next, the effect of STUB1 up-regulation on thrombosis was examined using 2-(4-hydroxy-3-methoxyphenyl)benzothiazole (YL-109) (Fig. 4E). YL-109, an analog of 2-(4-amino-3-methylphenyl)benzothiazole, is a preclinical compound with tumor-suppressive properties (*33*, *34*). Being a ligand of AHR, YL-109 binding to AHR elicits its nuclear translocation to induce the transcription of *STUB1* gene (*33*). In our model, YL-109 significantly (Hb, $P = 0.023$; LDH, $P = 0.017$) inhibited IS-induced thrombosis in the flow loops (Fig. 4F). Similarly, we observed a dose-dependent reduction in TF expression and activity along with doubling of STUB1 in vSMCs (Fig. 4, G and H, and fig. S4). Because YL-109 increases STUB1 expression, it is likely to enhance TF ubiquitination, which was examined using coexpression of ubiquitin and TF in the presence of uremic serum. YL-109 treatment increased the higher–molecular weight polyubiquitinated TF in vSMCs (Fig. 4I). Together, these genetic and pharmacological manipulations of STUB1 in vSMCs lining the flow loops consistently demonstrated a regulation of thrombosis by STUB1 in a cell type–specific manner.

IS-AHR-STUB1 axis modulation reverses the hyperthrombotic uremic phenotype to non-CKD range without altering hemostasis

We next examined whether augmented STUB1 suppressed the hyperthrombotic uremic milieu in vivo using the indolic solute–specific animal model (Fig. 1). The effects were compared to heparin, which is a standard-of-care antithrombotic in CKD patients (Fig. 5A). Compared to the IS group, YL-109 significantly ($P = 0.005$) prolonged the TtO (Fig. 5, B and C) with no differences in IS concentration between these groups (fig. S5A). Because STUB1-TF is a CKD-specific thrombotic pathway, we posited that its targeting by YL-109 is likely to revert the thrombogenicity to the non-CKD range. Therefore, we compared the effect of YL-109 to the probenecid (non-CKD) controls. The results showed no difference in TtO with IS + YL-109 compared to probenecid controls. On the other hand, heparin at a dose considered therapeutic in humans (*35*) significantly ($P = 0.001$) prolonged TtO compared to both IS and probenecid controls (Fig. 5C). YL-109–treated animals showed a significant increase in STUB1 ($P = 0.004$) and decrease in TF ($P = 0.001$) in their aortae (Fig. 5D and fig. S5B). To further probe a quantitative link between changes in TF expression and thrombogenicity in vivo, we correlated the reduction of TF in the aortic lysates of individual mice exposed to IS + YL-109 to the prolongation of TtO. We hypothesized that both these parameters will inversely correlate should the reduction in TF expression in the vessel wall reduce the thrombogenicity in the uremic milieu. A significant negative correlation (Spearman rho = −0.833 and $P = 0.02$) between the reduction in TF within the vessel wall and prolongation of TtO was observed in mice treated with YL-109 (Fig. 5E). Together, these data strongly suggest that reduction in TF by STUB1 regressed the hyperthrombotic uremic phenotype to the non-CKD range.

Because the solute-specific animal model partially recapitulates the uremic phenotype, these results warranted further validation in an established model of CKD. Among the different animal models of CKD, the proteinuric CKD model and hypertensive model are likely to confound the thrombosis assay due to loss of anti- and prothrombotic factors in the urine (*36*) and increased endothelin, respectively, in these models (*37*). Therefore, we used the adenine-induced renal injury model, a well-established model of uremia induced by extensive tubulointerstitial fibrosis (fig. S5C) (*38*). Within 2 weeks of 0.25% adenine diet, the animals showed significant ($P < 0.001$) increases in IS concentrations and blood urea nitrogen, corresponding to advanced CKD patients (Fig. 5F and fig. S5D). A significant ($P = 0.01$) reduction in TtO was observed in the adenine-induced CKD animals compared to animals on a regular chow diet (Fig. 5G), further supporting CKD as a hyperthrombotic environment. In the adenine-treated group, the TtO was significantly prolonged with CH223191 ($P = 0.004$) or YL-109 ($P = 0.050$), compared to the group treated with adenine alone (Fig. 5G), despite no differences in renal function between these three groups (fig. S5D). Furthermore, similar to the indolic solute–specific model (Fig. 5C), no differences in TtO were noted in the CH223191-treated ($P = 0.374$) and YL-109–treated ($P = 0.983$) groups when compared to the animals on a regular chow diet (non-CKD animals). All these data obtained from two independent models strongly argue for CKD as a hyperthrombotic milieu and indicate that uremia-induced thrombogenicity is normalized to a non-CKD range with the modulation of AHR-STUB1 axis.

The antithrombotic effects of the above agents were weighed against the bleeding risk using the standard tail vein transection model (*20*). Because STUB1 modulation normalized the thrombotic risk to non-CKD range, we compared YL-109–mediated alteration in bleeding time to probenecid (non-CKD) controls. The data showed no reduction in bleeding time with IS compared to probenecid controls (Fig. 5H). Compared to the probenecid controls, bleeding time was not different from YL-109 (Fig. 5H) and fell within the two SD ranges of the non-CKD controls' bleeding time (Fig. 5I, clear area). In contrast, heparin significantly ($P = 0.003$) prolonged the bleeding time beyond two SDs of probenecid controls (Fig. 5I, shaded area). Overall, these data indicate that, unlike heparin, STUB1 modulation reverted the IS-mediated hyperthrombotic phenotype to the nonuremic range without enhancing the bleeding risk.

DISCUSSION

CKD patients are prone to thrombosis and are specifically sensitive to the relatively CKD-nonspecific antithrombotic and antiplatelet agents (*12*, *13*). CKD patients are at fourfold increased risk of bleeding, which is further augmented by 50% with every 30 ml/min decrease in creatinine clearance (*39*, *40*). To some, this implies that a CKD patient represents an extreme case of classic vascular disease, and to others, this implies that the CKD milieu is distinct and unique. Our data support the latter and implicate IS in particular as a mediator of the hyperthrombotic uremic state through modulation of STUB1-TF interaction. Here, we show that reduced STUB1-TF interaction in vSMCs in uremia stabilizes TF and augments thrombosis upon exposure to vascular injury. Conversely, restoration of STUB1-TF interaction by suppression of uremic effect by AHR antagonist or STUB1 inducer augments TF ubiquitination and degradation and inhibits thrombosis. These data help discern the antithrombotic mechanism of AHR antagonism and add to the sophistication of the complex vascular biology of CKD while also highlighting the role of dynamic protein-protein interaction influenced by the uremic state, which we further substantiate in human vessels. We also demonstrate the prominent role of STUB1-TF axis in mediating CKD-specific thrombotic risk, which reverses to non-CKD range upon pharmacological targeting.

Although there can be different explanations to the dynamic interaction of STUB1 and TF, rapid modulation of this interaction with AHR

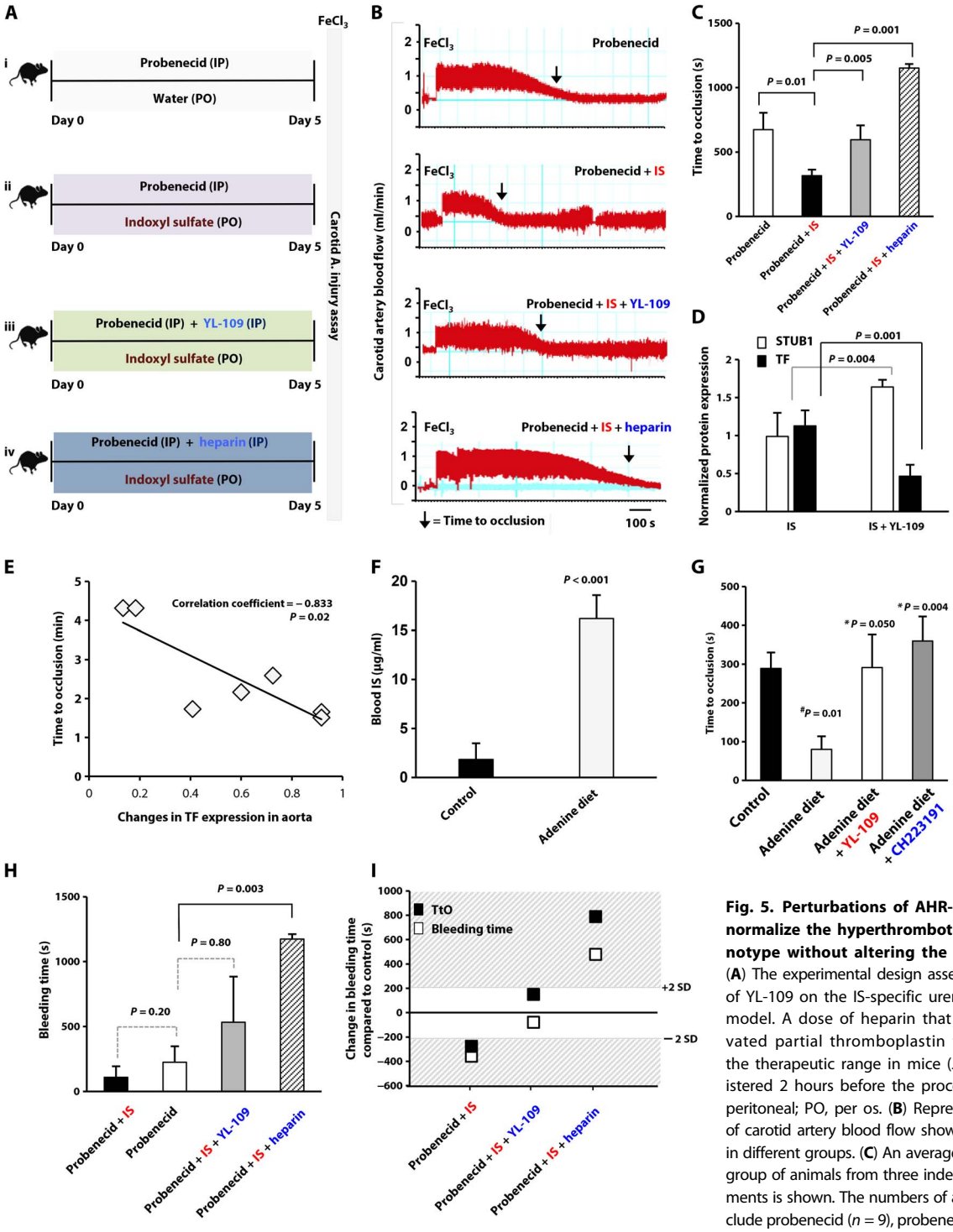

Fig. 5. Perturbations of AHR-STUB1-TF axis normalize the hyperthrombotic uremic phenotype without altering the bleeding risk. (**A**) The experimental design assessing the effect of YL-109 on the IS-specific uremic thrombosis model. A dose of heparin that increases activated partial thromboplastin time (aPTT) to the therapeutic range in mice (*35*) was administered 2 hours before the procedure. IP, intraperitoneal; PO, per os. (**B**) Representative traces of carotid artery blood flow showing TtO (arrow) in different groups. (**C**) An average TtO from each group of animals from three independent experiments is shown. The numbers of animals used include probenecid ($n = 9$), probenecid + IS ($n = 12$), probenecid + IS + YL-109 ($n = 8$), and probenecid + IS + heparin ($n = 6$). No difference in TtO was observed between probenecid and probenecid + IS + YL-109 ($P = 0.65$). Heparin significantly prolonged TtO compared to both IS and probenecid control groups ($P = 0.021$). Data are shown as means ± SD. (**D**) Mean normalized TF and STUB1 expression in the aortae of five mice injected with IS with or without YL-109 is shown. Student's *t* test was performed. Data are shown as means ± SD. (**E**) Changes in TF expression in the individual aortae of IS + YL-109–treated animals and their respective TtO are shown. A Spearman correlation analysis was performed. (**F**) IS concentrations in the blood of mice exposed to 0.25% adenine diet for 2 weeks and animals on regular chow (control) ($n = 5$ per group). Data are shown as means ± SD. (**G**) An average TtO in control (regular diet) and adenine-induced CKD mice with AHR inhibitor (CH223191) or STUB1 enhancer (YL-109) ($n = 5$ per group) is shown. $^{\#}P$ value compares the adenine and control groups. *P value compares CH223191 and YL-109 groups with the adenine group. Data are shown as means ± SEM. (**H**) Average tail vein bleeding times for each group ($n = 5$ per group). Data are shown as means ± SD. (**I**) Differences in the average tail vein bleeding times (*y* axis) between probenecid control (non-CKD) and other groups (CKD). The solid line represents the average bleeding time of the control group, and the dotted lines represent two SDs of bleeding time from the control group. The shaded areas are the regions beyond 2 SD.

status argues for the role of AHR and posttranslational modifications (PTMs) in this process. Because STUB1, AHR (*24*), and TF bind to each other (*11*), it is likely that they form a multiprotein complex, which may undergo stoichiometric or conformational changes upon AHR activation (IS treatment) or AHR suppression (AHR antagonist treatment), altering the interactions between the components (*24*). The kinetics of STUB1-TF interaction support PTMs in either or both partners. Similar PTMs can modulate the interaction of STUB1 with other targets (*41*). This rapid STUB1-TF interaction is followed by ubiquitination and proteasomal degradation of TF, such that TF protein reaches its half-life within 40 min in vSMCs (*11*). The involvement of ubiquitination in regulating TF imparts specificity and efficiency to TF biology. This system is built for amplification, such that the target (TF), the ubiquitin ligase (STUB1), and the modifying protein (ubiquitin) are all governed by complex autoregulatory and pararegulatory loops (*26*). It is such a system that can regulate the biology of a central stimulus like TF, which is released and/or exposed on vSMCs early after vascular injury and especially within the context of the complex uremic milieu (*8*, *11*, *18*). Such biochemistry also explains why modest changes in any of the involved elements induce large, nonlinear effects on outcomes and a strong in vivo correlation between the reduction in thrombogenicity and changes in TF within the vessel wall in response to pharmacological manipulation of STUB1.

Even minor changes in TF expression are expected to have a substantial effect on thrombosis, because vessel wall TF activation is only a primary trigger, followed by a multitude of nonlinear and interrelated events, such as the extrinsic coagulation cascade and platelet aggregation (*42*), all of which amplify the primary trigger of TF activation to produce robust thrombus formation. Thus, perturbation of TF through the AHR-STUB1 axis represents an effective therapeutic strategy in CKD patients, because none of the current antithrombotics or the investigational agents such as factor XII and XI inhibitors target CKD-specific thrombosis (*14*, *15*). Their suboptimum efficacy is likely to be exacerbated by poor thrombus control from a persistent nidus of exposed vSMCs secondary to compromised reendothelialization of the vascular wound in the uremic milieu (*43*). Compounding the poor efficacy profile is their enhanced bleeding risk due to altered pharmacokinetics in CKD and perturbation of critical hemostatic defenses (*12*, *13*).

Two complementary in vivo thrombosis models used here, involving damaged endothelium, established the relevance of our in vitro studies. The added value of a solute-specific animal model in the context of vascular injury was in allowing us to directly address CKD-associated risk assessment. In addition to avoiding confounders such as hypertension in other CKD models (*16*), this animal model allows titration of a specific uremic solute to examine its effect at different stages of CKD. Although this animal model should be a valuable tool for mechanistic probing and is potentially useful in preclinical drug development, especially having been validated with an established adenine-induced CKD model, it does not emulate the human arterial rheological patterns or the flow characteristics that are critical in postinterventional thrombosis (*44*). The flow-loop system used herein (*32*) is a model of postinterventional thrombosis combining a humanized system of human cells and human blood simulating human coronary flow patterns. Clot formation in this system is defined by three discrete components, which provide a different view of the net extent of thrombosis. Hb and LDH measurements represent red cell content and active remodeling of the clot, respectively, and visual inspection assesses overall clot burden. The results from the flow loops tracked well with the genetic loss of function of STUB1 and with pharmacological up-regulation of STUB1. Interrogating the AHR-TF-STUB1-TF axis using orthogonal models has strengthened the translational relevance of this study.

We identified two discrete mechanisms of TF down-regulation in the uremic milieu, namely, increasing STUB1 concentration and enhanced STUB1-TF interaction, supporting the development of direct STUB1 activators and selective AHR modulators (sAHRMs) as antithrombotics (*45*). Because the effects of these agents are likely to be influenced by the state of AHR signaling, a biomarker based on the concentrations of uremic solutes (*11*) should further refine the risk-benefit profile for antithrombotics in CKD patients. Moreover, combining therapy with agents that target disease-specific mechanisms to normalize the uremic hyperthrombotic milieu together with the current antiplatelet/antithrombotic agents might enhance therapeutic efficacy and safety.

We recognize the study's limitations, knowing that thrombosis is a dynamic process orchestrated by several different cell types and mediators, and almost all of these components are altered in CKD (*3*, *4*). Although vessel wall factors and platelets in IS-mediated thrombosis are being examined (*11*, *18*, *46*), the roles of other metabolites (termed "thrombolome") (*3*, *11*), microvesicles, etc. remain to be probed to fully characterize the hyperthrombotic uremic milieu. Although the current report demonstrates the role of IS-AHR-STUB1 axis in suppressing TF, a potential ability of this axis to regulate other members of the coagulation cascade or platelets cannot be ruled out. Finally, YL-109 was developed as an sAHRM (*33*, *45*), but it may have additional effects on thrombosis through pathways other than AHR-STUB1-TF, and this warrants further investigation.

Several dynamic events influence thrombosis and hemostasis processes, and their precise quantification is required to determine the global thrombosis risk and allow individualization of therapy. CKD-specific thrombosis risk assessment can be performed by integrating these uremic solutes with conventional thrombotic markers (*3*, *11*, *12*). A combination of such a risk panel with a means of targeting CKD-specific thrombotic mediators is likely to improve the antithrombotic management in these patients. Our study focused on postinterventional thrombosis in CKD, because these patients carry high cardiovascular disease burden requiring complex vascular procedures and are also at risk of thrombosis of dialysis access, a lifeline of CKD patients. The signaling axis we identified needs further probing in other models of thrombosis.

MATERIALS AND METHODS

Study design

The number of animals was guided by the expected effect size and SD of the readout (TtO) to obtain 90% power at an α of 0.05. Male and female mice were randomized to different groups in these experiments. Although the administration of compounds in animal experiments was not performed in a blinded manner, an investigator blinded to the experimental groups performed the thrombosis assays.

Statistical analysis

Summary statistics are presented as the mean and SD or SEM. Analysis of variance (ANOVA), paired or unpaired Student's *t* test, or Wilcoxon rank sum test was used to compare the groups as appropriate, and the test for each experiment is indicated in the figure legends. A Spearman or Pearson correlation was performed to analyze the correlation between two variables, as appropriate. $P < 0.05$ was considered statistically significant.

SUPPLEMENTARY MATERIALS

www.sciencetranslationalmedicine.org/cgi/content/full/9/417/eaam8475/DC1
Materials and Methods
Fig. S1. An indolic solute–specific animal model.
Fig. S2. STUB1 regulation of TF protein.
Fig. S3. STUB1 interaction with TF.
Fig. S4. STUB1 expression in the YL-109–treated flow loops.
Fig. S5. AHR or STUB1 manipulation in uremic animal model.
Table S1. Demographic and clinical characteristics of patients included in the study to examine the vascular expression of STUB1 and TF.

REFERENCES AND NOTES

1. G. Ocak, K. J. van Stralen, F. R. Rosendaal, M. Verduijn, P. Ravani, R. Palsson, T. Leivestad, A. J. Hoitsma, M. Ferrer-Alamar, P. Finne, J. De Meester, C. Wanner, F. W. Dekker, K. J. Jager, Mortality due to pulmonary embolism, myocardial infarction, and stroke among incident dialysis patients. *J. Thromb. Haemost.* **10**, 2484–2493 (2012).
2. I. Iakovou, T. Schmidt, E. Bonizzoni, L. Ge, G. M. Sangiorgi, G. Stankovic, F. Airoldi, A. Chieffo, M. Montorfano, M. Carlino, I. Michev, N. Corvaja, C. Briguori, U. Gerckens, E. Grube, A. Colombo, Incidence, predictors, and outcome of thrombosis after successful implantation of drug-eluting stents. *JAMA* **293**, 2126–2130 (2005).
3. M. Shashar, J. Francis, V. Chitalia, Thrombosis in the uremic milieu—Emerging role of "thrombolome." *Semin. Dial.* **28**, 198–205 (2015).
4. L. F. Casserly, L. M. Dember, Thrombosis in end-stage renal disease. *Semin. Dial.* **16**, 245–256 (2003).
5. M. A. Crowther, C. M. Clase, P. J. Margetts, J. Julian, K. Lambert, D. Sneath, R. Nagai, S. Wilson, A. J. Ingram, Low-intensity warfarin is ineffective for the prevention of PTFE graft failure in patients on hemodialysis: A randomized controlled trial. *J. Am. Soc. Nephrol.* **13**, 2331–2337 (2002).
6. V. I. Patel, S. Mukhopadhyay, J. M. Guest, M. F. Conrad, M. T. Watkins, C. J. Kwolek, G. M. LaMuraglia, R. P. Cambria, Impact of severe chronic kidney disease on outcomes of infrainguinal peripheral arterial intervention. *J. Vasc. Surg.* **59**, 368–375 (2014).
7. S. H. Park, W. Kim, C. S. Park, W. Y. Kang, S. H. Hwang, A comparison of clopidogrel responsiveness in patients with versus without chronic renal failure. *Am. J. Cardiol.* **104**, 1292–1295 (2009).
8. V. C. Chitalia, S. Shivanna, J. Martorell, M. Balcells, I. Bosch, K. Kolandaivelu, E. R. Edelman, Uremic serum and solutes increase post-vascular interventional thrombotic risk through altered stability of smooth muscle cell tissue factor. *Circulation* **127**, 365–376 (2013).
9. M. B. Taubman, L. Wang, C. Miller, The role of smooth muscle derived tissue factor in mediating thrombosis and arterial injury. *Thromb. Res.* **122** (suppl. 1), S78–S81 (2008).
10. R. Vanholder, E. Schepers, A. Pletinck, E. V. Nagler, G. Glorieux, The uremic toxicity of indoxyl sulfate and p-cresyl sulfate: A systematic review. *J. Am. Soc. Nephrol.* **25**, 1897–1907 (2014).
11. S. Shivanna, K. Kolandaivelu, M. Shashar, M. Belghasim, L. Al-Rabadi, M. Balcells, A. Zhang, J. Weinberg, J. Francis, M. P. Pollastri, E. R. Edelman, D. H. Sherr, V. C. Chitalia, The aryl hydrocarbon receptor is a critical regulator of tissue factor stability and an antithrombotic target in uremia. *J. Am. Soc. Nephrol.* **27**, 189–201 (2016).
12. D. I. Jalal, M. Chonchol, G. Targher, Disorders of hemostasis associated with chronic kidney disease. *Semin. Thromb. Hemost.* **36**, 34–40 (2010).
13. S. S. Basra, P. Tsai, N. M. Lakkis, Safety and efficacy of antiplatelet and antithrombotic therapy in acute coronary syndrome patients with chronic kidney disease. *J. Am. Coll. Cardiol.* **58**, 2263–2269 (2011).
14. T. David, Y. C. Kim, L. K. Ely, I. Rondon, H. Gao, P. O'Brien, M. W. Bolt, A. J. Coyle, J. L. Garcia, E. A. Flounders, T. Mikita, S. R. Coughlin, Factor XIa-specific IgG and a reversal agent to probe factor XI function in thrombosis and hemostasis. *Sci. Transl. Med.* **8**, 353ra112 (2016).
15. T. Petzold, M. Thienel, I. Konrad, I. Schubert, R. Regenauer, B. Hoppe, M. Lorenz, A. Eckart, S. Chandraratne, C. Lennerz, C. Kolb, D. Braun, J. Jamasbi, R. Brandl, S. Braun, W. Siess, C. Schulz, S. Massberg, Oral thrombin inhibitor aggravates platelet adhesion and aggregation during arterial thrombosis. *Sci. Transl. Med.* **8**, 367ra168 (2016).
16. H. C. Yang, Y. Zuo, A. B. Fogo, Models of chronic kidney disease. *Drug Discov. Today Dis. Models* **7**, 13–19 (2010).
17. T. Kokubo, N. Ishikawa, H. Uchida, S. E. Chasnoff, X. Xie, S. Mathew, K. A. Hruska, E. T. Choi, CKD accelerates development of neointimal hyperplasia in arteriovenous fistulas. *J. Am. Soc. Nephrol.* **20**, 1236–1245 (2009).
18. B. Gondouin, C. Cerini, L. Dou, M. Sallée, A. Duval-Sabatier, A. Pletinck, R. Calaf, R. Lacroix, N. Jourde-Chiche, S. Poitevin, L. Arnaud, R. Vanholder, P. Brunet, F. Dignat-George, S. Burtey, Indolic uremic solutes increase tissue factor production in endothelial cells by the aryl hydrocarbon receptor pathway. *Kidney Int.* **84**, 733–744 (2013).
19. S. K. Nigam, K. T. Bush, G. Martovetsky, S.-Y. Ahn, H. C. Liu, E. Richard, V. Bhatnagar, W. Wu, The organic anion transporter (OAT) family: A systems biology perspective. *Physiol. Rev.* **95**, 83–123 (2015).
20. S. Matsuura, R. Mi, M. Koupenova, A. Eliades, S. Patterson, P. Toselli, J. Thon, J. E. Italiano Jr., P. C. Trackman, N. Papadantonakis, K. Ravid, Lysyl oxidase is associated with increased thrombosis and platelet reactivity. *Blood* **127**, 1493–1501 (2016).
21. D. Kirchhofer, P. Moran, S. Bullens, F. Peale, S. Bunting, A monoclonal antibody that inhibits mouse tissue factor function. *J. Thromb. Haemost.* **3**, 1098–1099 (2005).
22. J. T. Paz, C. A. Christian, I. Parada, D. A. Prince, J. R. Huguenard, Focal cortical infarcts alter intrinsic excitability and synaptic excitation in the reticular thalamic nucleus. *J. Neurosci.* **30**, 5465–5479 (2010).
23. Y. Miao, Z. Yu-Jie, W. Zhi-Jian, S. Dong-Mei, L. Yu-Yang, Z. Ying-Xin, G. Fei, Y. Shi-Wei, J. De-An, Chronic kidney disease and the risk of stent thrombosis after percutaneous coronary intervention with drug-eluting stents. *Catheter. Cardiovasc. Interv.* **80**, 361–367 (2012).
24. J. L. Morales, G. H. Perdew, Carboxyl terminus of hsc70-interacting protein (CHIP) can remodel mature aryl hydrocarbon receptor (AhR) complexes and mediate ubiquitination of both the AhR and the 90 kDa heat-shock protein (hsp90) in vitro. *Biochemistry* **46**, 610–621 (2007).
25. Q. Dai, C. Zhang, Y. Wu, H. McDonough, R. A. Whaley, V. Godfrey, H.-H. Li, N. Madamanchi, W. Xu, L. Neckers, D. Cyr, C. Patterson, CHIP activates HSF1 and confers protection against apoptosis and cellular stress. *EMBO J.* **22**, 5446–5458 (2003).
26. A. Ciechanover, The unravelling of the ubiquitin system. *Nat. Rev. Mol. Cell Biol.* **16**, 322–324 (2015).
27. M. T. Kirber, K. Chen, J. F. Keaney Jr., YFP photoconversion revisited: Confirmation of the CFP-like species. *Nat. Methods* **4**, 767–768 (2007).
28. C. A. Ballinger, P. Connell, Y. Wu, Z. Hu, L. J. Thompson, L.-Y. Yin, C. Patterson, Identification of CHIP, a novel tetratricopeptide repeat-containing protein that interacts with heat shock proteins and negatively regulates chaperone functions. *Mol. Cell. Biol.* **19**, 4535–4545 (1999).
29. E. K. Spicer, R. Horton, L. Bloem, R. Bach, K. R. Williams, A. Guha, J. Kraus, T.-C. Lin, Y. Nemerson, W. H. Konigsberg, Isolation of cDNA clones coding for human tissue factor: Primary structure of the protein and cDNA. *Proc. Natl. Acad. Sci. U.S.A.* **84**, 5148–5152 (1987).
30. M. C. Riella, P. Roy-Chaudhury, Vascular access in haemodialysis: Strengthening the Achilles' heel. *Nat. Rev. Nephrol.* **9**, 348–357 (2013).
31. S. Moshe, J. Siwak, U. Tapan, S. Y. Lee, R. D. Meyer, P. Parrack, J. Tan, F. Khatami, J. Francis, Q. Zhao, K. Hartshorn, V. B. Kolachalama, N. Rahimi, V. Chitalia, c-Cbl mediates the degradation of tumorigenic nuclear β-catenin contributing to the heterogeneity in Wnt activity in colorectal tumors. *Oncotarget* **7**, 71136–71150 (2016).
32. K. Kolandaivelu, B. B. Leiden, E. R. Edelman, Predicting response to endovascular therapies: Dissecting the roles of local lesion complexity, systemic comorbidity, and clinical uncertainty. *J. Biomech.* **47**, 908–921 (2014).
33. H. Hiyoshi, N. Goto, M. Tsuchiya, K. Iida, Y. Nakajima, N. Hirata, Y. Kanda, K. Nagasawa, J. Yanagisawa, 2-(4-Hydroxy-3-methoxyphenyl)-benzothiazole suppresses tumor progression and metastatic potential of breast cancer cells by inducing ubiquitin ligase CHIP. *Sci. Rep.* **4**, 7095 (2014).
34. T. D. Bradshaw, M. C. Bibby, J. A. Double, I. Fichtner, P. A. Cooper, M. C. Alley, S. Donohue, S. F. Stinson, J. E. Tomaszewjski, E. A. Sausville, M. F. G. Stevens, Preclinical evaluation of amino acid prodrugs of novel antitumor 2-(4-amino-3-methylphenyl)benzothiazoles. *Mol. Cancer Ther.* **1**, 239–246 (2002).
35. Y. Li, J.-F. Sun, X. Cui, H. Mani, R. L. Danner, X. Li, J.-W. Su, Y. Fitz, P. Q. Eichacker, The effect of heparin administration in animal models of sepsis: A prospective study in *Escherichia coli*-challenged mice and a systematic review and metaregression analysis of published studies. *Crit. Care Med.* **39**, 1104–1112 (2011).
36. J. Loscalzo, Venous thrombosis in the nephrotic syndrome. *N. Engl. J. Med.* **368**, 956–958 (2013).
37. A. Bertelli, A. A. Bertelli, G. Galmozzi, L. Giovannini, M. Mian, Thrombosis induced by endothelin (ET-1) and carrageenin in rats treated with indomethacin and propionyl carnitine. *Drugs Exp. Clin. Res.* **19**, 75–78 (1993).
38. T. Jia, H. Olauson, K. Lindberg, R. Amin, K. Edvardsson, B. Lindholm, G. Andersson, A. Wernerson, Y. Sabbagh, S. Schiavi, T. E. Larsson, A novel model of adenine-induced tubulointerstitial nephropathy in mice. *BMC Nephrol.* **14**, 116 (2013).
39. K. A. A. Fox, E. M. Antman, G. Montalescot, S. Agewall, B. SomaRaju, F. W. A. Verheugt, J. Lopez-Sendon, H. Hod, S. A. Murphy, E. Braunwald, The impact of renal dysfunction on outcomes in the ExTRACT-TIMI 25 trial. *J. Am. Coll. Cardiol.* **49**, 2249–2255 (2007).
40. K. P. Alexander, A. Y. Chen, M. T. Roe, L. K. Newby, C. M. Gibson, N. M. Allen-LaPointe, C. Pollack, W. B. Gibler, E. M. Ohman, E. D. Peterson; CRUSADE Investigators, Excess dosing of antiplatelet and antithrombin agents in the treatment of non-ST-segment elevation acute coronary syndromes. *JAMA* **294**, 3108–3116 (2005).
41. P. Muller, E. Ruckova, P. Halada, P. J. Coates, R. Hrstka, D. P. Lane, B. Vojtesek, C-terminal phosphorylation of Hsp70 and Hsp90 regulates alternate binding to co-chaperones CHIP and HOP to determine cellular protein folding/degradation balances. *Oncogene* **32**, 3101–3110 (2013).

42. N. Mackman, Triggers, targets and treatments for thrombosis. *Nature* **451**, 914–918 (2008).
43. L. Dou, E. Bertrand, C. Cerini, V. Faure, J. Sampol, R. Vanholder, Y. Berland, P. Brunet, The uremic solutes p-cresol and indoxyl sulfate inhibit endothelial proliferation and wound repair. *Kidney Int.* **65**, 442–451 (2004).
44. U. Windberger, A. Bartholovitsch, R. Plasenzotti, K. J. Korak, G. Heinze, Whole blood viscosity, plasma viscosity and erythrocyte aggregation in nine mammalian species: Reference values and comparison of data. *Exp. Physiol.* **88**, 431–440 (2003).
45. I. A. Murray, G. Krishnegowda, B. C. DiNatale, C. Flaveny, C. Chiaro, J.-M. Lin, A. K. Sharma, S. Amin, G. H. Perdew, Development of a selective modulator of aryl hydrocarbon (Ah) receptor activity that exhibits anti-inflammatory properties. *Chem. Res. Toxicol.* **23**, 955–966 (2010).
46. K. Yang, C. Du, X. Wang, F. Li, Y. Xu, S. Wang, S. Chen, F. Chen, M. Shen, M. Chen, M. Hu, T. He, Y. Su, J. Wang, J. Zhao, Indoxyl sulfate induces platelet hyperactivity and contributes to chronic kidney disease-associated thrombosis in mice. *Blood* **129**, 2667–2679 (2017).
47. A. Zhang, K. Rijal, S. Kah Ng, K. Ravid, V. Chitalia, A mass spectrometric method for quantification of tryptophan-derived uremic solutes in human serum. *J. Biol. Methods* **4**, e75 (2017).

Acknowledgments: We acknowledge N. Mackman (University of North Carolina, Chapel Hill) for his guidance in TF activity assay and D. Salant and N. Rahimi (Boston University School of Medicine) for sharing resources and cell lines. We thank C. Patterson (University of North Carolina, Chapel Hill) for STUB1 KO and knockin (KI) MEFs and WT and H260Q STUB1 constructs. We also thank F. García Polite, D. Gómez Jiménez, and F. Lozano (Universitat Ramon Llull, Barcelona, Spain and Massachusetts Institute of Technology) for their technical assistance in flow-loop experiments and D. Mun for the help in obtaining patient data. We also thank M. Kirber at the Boston University Medical Center (BUMC) Core facilities for his assistance in confocal microscopy. Portions of this work were presented at the 2015 and 2016 American Society of Nephrology meetings. **Funding:** This work was funded in part by NIH R01 HL132325 and R01 CA175382; Evans Faculty Merit award (V.C.C.); NIH R01 HL080442 (K. Ravid); National Institute of General Medical Sciences (NIGMS) R01 GM49039 (E.R.E.); P42 ES007381 and the Art BeCAUSE Breast Cancer Foundation (D.H.S.); Hariri Research Award (no. 2016-10-009) from the Hariri Institute of Computing, Boston University and American Heart Association's Scientist Development grant no. 17SDG33670323 (V.B.K.); Sharon Anderson Research Fellowship grant award from the American Society of Nephrology (M.S.); AHA Fellow to Faculty Transition grant 12FTF12080241 (K.K.); the grant SAF2013-43302-R from Spain Ministerio de Economía y Competitividad and Fundació Empreses IQS (M.B.); T32 training in renal biology T32 DK007053-44 (K. Rijal); and T32 training grant in cardiovascular biology T32 HL007224-40 (J.W.). A part of this work was funded by the Thrombosis and Hemostasis Affinity Research Collaborative program from the Department of Medicine, BUMC. **Author contributions:** V.C.C. and M.S. designed the research and experiments, with contributions from K. Ravid; M.S., J.W., S.R., F.A., K. Rijal, and S.R. performed the cell-based experiments; J.M.H. and M.E.B. performed immunofluorescence studies; M.S., M.E.B., S.M., J.W., S.R., and F.A. performed the animal experiments; J.F., J.M.H., and A.G. performed the analysis on AVF and immunofluorescence data; K.K. and M.B. designed and performed the flow-loop experiments; V.B.K. performed quantitative histology and image processing; M.O. and K.N. synthesized YL-109; D.K. provided anti-TF neutralizing antibody; R.R. assisted in the photochemical thrombosis injury model; V.C.C. and M.S. reviewed and analyzed the final data; M.S., M.E.B., and V.C.C. prepared the figures and manuscript; D.K., D.H.S., J.F., S.M., J.M.H., K.K., V.B.K., R.R., E.R.E., and K. Ravid contributed conceptually to different degrees and edited the manuscript. **Competing interests:** The authors declare that they have no competing interests.

Submitted 24 January 2017
Resubmitted 31 July 2017
Accepted 4 October 2017
Published 22 November 2017
10.1126/scitranslmed.aam8475

Citation: M. Shashar, M. E. Belghasem, S. Matsuura, J. Walker, S. Richards, F. Alousi, K. Rijal, V. B. Kolachalama, M. Balcells, M. Odagi, K. Nagasawa, J. M. Henderson, A. Gautam, R. Rushmore, J. Francis, D. Kirchhofer, K. Kolandaivelu, D. H. Sherr, E. R. Edelman, K. Ravid, V. C. Chitalia, Targeting STUB1–tissue factor axis normalizes hyperthrombotic uremic phenotype without increasing bleeding risk. *Sci. Transl. Med.* **9**, eaam8475 (2017).

Science Translational Medicine
AAAS

www.sciencetranslationalmedicine.org/cgi/content/full/9/417/eaam8475/DC1

Supplementary Materials for

Targeting STUB1–tissue factor axis normalizes hyperthrombotic uremic phenotype without increasing bleeding risk

Moshe Shashar, Mostafa E. Belghasem, Shinobu Matsuura, Joshua Walker, Sean Richards, Faisal Alousi, Keshab Rijal, Vijaya B. Kolachalama, Mercedes Balcells, Minami Odagi, Kazuo Nagasawa, Joel M. Henderson, Amitabh Gautam, Richard Rushmore, Jean Francis, Daniel Kirchhofer, Kumaran Kolandaivelu, David H. Sherr, Elazer R. Edelman, Katya Ravid, Vipul C. Chitalia*

*Corresponding author. Email: vichital@bu.edu

Published 22 November 2017, *Sci. Transl. Med.* **9**, eaam8475 (2017)
DOI: 10.1126/scitranslmed.aam8475

This PDF file includes:

Materials and Methods

Human subjects and serum collection: Pooled uremic sera of ESRD patients on hemodialysis and age-, gender- and ethnic background-matched control sera were described previously *(8)*. Briefly, ERSD patients on hemodialysis (HD) were recruited randomly from a pool of 150 patients at the DaVita Hemodialysis Center (Boston, MA). The protocol was approved by Institutional Review Boards of Boston University Medical Center and Massachusetts Institute of Technology. Informed consents were obtained and 10 ml of blood collected before a HD session. Patients with Hb < 8 gm/dl were excluded. Control sera for age-, gender- and ethnicity-matched subjects were obtained from Research Blood Component Inc. Controls with creatinine >1.0 mg/dl were excluded.

Generation of an indolic solute-specific thrombosis model: C57BL/6 male and female mice (10-14 weeks old) were given IS ad libitum in water, and the excretion of IS was inhibited by probenecid, an OAT1 and OAT3 channel inhibitor. Different protocols combining IS administration with probenecid were examined. IS dissolved in drinking water at 4 mg/ml and probenecid at 15 mg/kg IP twice daily yielded consistently high IS above 40-50 μg/ml, concentrations similar to patients with CKD stage 5/ESRD (*11*), and was thus chosen for subsequent experiments. Serum IS concentrations were measured on days 0, 2, and 5 using LC/MS developed and validated for the measurement of IS *(45)*, after which the animals were subjected to ferric chloride-mediated carotid injury, performed as previously described *(20)*. Briefly, the right carotid artery was exposed in isoflurane-anesthetized animals, and basal blood flow was recorded before and after 1 min placement of a ferric chloride ($FeCl_3$)-soaked filter paper under the artery. The TtO was determined as time until the first measurement between 0 and 0.29 ml/min, which corresponds to total occlusion of the lumen (**Fig. 1C**). Basal blood flow was defined as the average of 30 sec of measurements before filter paper placement.

For histological analysis of thrombi, carotid artery thrombi were induced as described above with $FeCl_3$, and a 3-5 mm cranially located portion of the artery was collected, fixed, embedded in paraffin, and serially sectioned (10 μm) over its entire length, resulting in 100-300 sections per animal. Images of hematoxylin and eosin-stained sections were acquired using an Eclipse 50i microscope equipped with an Insight2 camera and SPOT imaging software v5.0 (SPOT Imaging).

Different concentrations of $FeCl_3$ were screened, and the one that resulted in TtO with minimum variation was chosen for further experiments (**fig. S1F**). The effects of the AHR antagonist and YL-109 were examined in the following groups – probenecid (control), IS + probenecid, and IS + YL-109 (5 mg/kg IP) or CH223191 (10 mg/kg IP). Both YL-109 and CH223191 suspended in DMSO were further dissolved in vegetable oil before IP injection. For the group treated with heparin**,** the animals received a single dose of heparin given 2 hours before the procedure (500 units/kg), which is known to prolong aPTT to within the therapeutic range (1.5-2.5 times control) *(33)*.

Image processing algorithm developed to quantify STUB1 and TF expression in human tissues: We developed an object recognition pipeline to correlate cell-level intensity distribution of TF with STUB1 (**Fig. 3H**). The pipeline consisted of image pre-processing, size-based morphology filtering, and object-level intensity correlation. Grayscale images were generated from the original TF and STUB1 images and converted to binary images using Otsu's method *(29),* and a flood-fill operation was performed on background pixels of the binary images to fill local image regions or holes. Binary erosion followed by dilation of the flood-filled binary images were performed using a disc-shaped morphological structuring element of 5-pixel radius, resulting in a set of connected components (image objects) along with corresponding object-level properties. For each image object in the processed TF image, the closest object within the processed STUB1 image was identified by comparing pairwise Euclidean distances between the objects within the 2 images. Area-averaged mean (AAM) intensity values for each image

object were then computed followed by image-level averaging of all the AAM values to correlate STUB1 distribution with TF across several images (**Fig. 3G-3K**).

Pixel-level STUB1-TF colocalization algorithm: Grayscale images were generated from the original TF and STUB1 images, followed by computation of image-level thresholds using Otsu's method *(29)*. Percent colocalization was defined as the fraction of pixels with intensity values greater than image-specific thresholds for both the images. The difference in the extent of pixel-level colocalization per image was first computed in uremic vessels and compared to that in non-uremic vessels.

Flow-loop system: Flow-loops consisting of silastic tubes coated with primary aortic human vSMCs or STUB1 KO or WT MEFs cells were subjected to coronary flow conditions that emulate the endovascular intervention ex vivo. Before cell seeding, 4-cm-long, 1/8" ID Tygon tubes (Saint-Gobain) were prepared and injected with 100,000 cells/ml vSMCs *(8,11)*. The tubes were then cultured for 16 hours under axial rotation at 10 rph, 37°C, 5% CO_2. vSMC-coated tubes were exposed to uremic serum (5%) or IS (10 μM) with or without 25 μM YL-109 for 24 hours. The segments were explanted, and positioned in the reactive site flow loop model as described (**Fig. 4A-4B**) *(11)*. Fresh whole blood was collected from healthy volunteers in a 10% acid-citrate dextrose solution. Immediately before testing, a 100 mM $CaCl_2$/75 mM $MgCl_2$ solution was added to the blood (70 ml solution per 1 ml blood) and loaded into the flow loops. After 10-minute runs, the loops were emptied and flushed with 60 ml Tyrodes buffer (0.01 M HEPES, 0.75 mM $MgCl_2$) followed by visual inspection of the clot and its lysis. The clot was lysed with 1% Triton-X solution for 20 minutes. LDH and Hb were measured using Quantichrom Assays.

Thrombosis in a flow loop system is a binary event that can further be defined by three discrete components. The Hb and LDH measurements represent the clot burden based on red cell content in the former and lysis of the clot in the latter. Each provides a different view of net clot burden.

Adenine-induced CKD model: A group of 10- to 14-week-old mixed male and female C57BL/6 wild-type mice (Jackson Laboratories) were fed a normal chow diet (Teklad Global 18% Protein Rodent Diet, Envigo) supplemented with 0.25% adenine (vitamin B4; diet formulated by Research Diets) for 14 days. Control animals were fed with normal chow diet. Additional mice exposed to the adenine-supplemented diet were treated with STUB1 inducer, YL-109 (5 mg/kg), or the AHR antagonist CH223191 (10 mg/kg) for 5 days starting at day 10 of exposure to the adenine diet. The animals were subjected to the thrombosis assay at the end of the study period as described above. Blood urea nitrogen (BUN) in these animals was determined using the QuantiChrom Urea Assay Kit (DIUR-100) (BioAssay Systems) by measuring the concentration of BUN in plasma, following the manufacturer's standard protocol. IS concentrations were determined using a pre-validated LC/MS method at the Metabolomics Core at Boston University Medical Center *(45)*.

Photochemical model of thrombosis: A group of 10- to 14-week-old male and female C57/BL6J wild type were treated for a total of 5 days with IS (ad libitum, 4 mg/mL in water) and probenecid (150 mg/kg) (intraperitoneal, twice daily). After treatment, the animals were subjected to a photochemical injury model modified as below *(22)*. Carotid artery thrombosis was induced by administration of Rose Bengal (4,5,6,7-tetrachloro-2',4',5',7'-tetraiodofluorescein) (Sigma). Instead of the tail vein, a single dose of 100 µL of Rose Bengal (25 mg/mL) was injected slowly over 2 minutes in the pre-cannulated external jugular vein. This modification provided an access to a larger vessel compared to the tail vein and allowed repeated Rose Bengal dye injections under controlled manner through a vessel, which was already exposed during surgery. The carotid artery was exposed to white light from a 3 mm diameter fiber optic cable connected to 200 W illuminator (Dolan Jenner Industries). The optical system was designed to have an emission spectrum that encompassed the in vivo absorption range of Rose Bengal (maximum absorbance at 562 nm). The carotid blood flow was determined using 0.5PSB S-series flowprobe connected to a TS420 perivascular transit-time

flowmeter (Transonic) and the time to reduction of carotid blood flow to baseline to 0-0.2 ml/min was considered as TtO.

Anti-TF neutralizing antibody assay: A group of 10- to 14-week-old male and female C57Bl6/J wild-type mice was exposed to probenecid + IS for five days as described above, followed by $FeCl_3$ carotid artery thrombosis assay. Half an hour before the thrombosis assay, the animals were given one dose of isotype-matched control antibody injected IP (20 mg/kg rat anti-mouse; IgG2A; eBioscience) and rat anti-mouse anti-TF neutralizing antibody (20 mg/kg) *(21)*.

Tail vein bleeding test: The tail vein bleeding time was determined as described previously *(20)*. Tails of anesthetized C57BL/6 mice (12-16 weeks old) were transected 5 mm from the tip with a razor blade. The tail was immersed in a 15 ml tube containing 13 ml of PBS prewarmed to 37°C. Bleeding times were determined when the bleeding stopped for 20 seconds.

Cell culture, cell lysis, immunoblotting, immunoprecipitation, and immunofluorescence: Primary vSMCs were grown in low-glucose DMEM medium + 5% calf serum + 1% penicillin and streptomycin + 1% L-glutamine. HEK293T and HUVEC-tert cells were grown in high DMEM + 10% FBS and 1% penicillin and streptomycin. Cell harvest and immunoblotting have been described previously *(8)*. STUB1 KO mouse embryonic fibroblasts MEF's, a gift from Dr. C. Patterson's lab (UNC, Chapel Hill), were grown in DMEM high glucose with 10% FBS and 1% penicillin and streptomycin. Monoclonal antibodies specific for tissue factor HTF1 (Thermo Fisher Scientific), GAPDH, MYC and FLAG tags (Cell Signaling), and STUB1 (Santa Cruz) were used. Immunoprecipitation assays were performed using antibody treatment followed by agarose (A+G plus) beads (Santa Cruz), as described previously *(8)*. The vSMCs grown in chamber slides (Lab-Tek) were fixed with methanol and processed as described previously using Leica SP5 confocal microscopy *(8)*.

Plasmid constructs: All STUB1 constructs were generously provided by Dr. Cam Patterson's laboratory at the University of North Carolina, Chapel Hill. The C-terminus FLAG-tagged TF

constructs were generated by cloning human TF in pQCXIP vector (Clontech) at NotI and BamHI sites. The primer sequences including C-terminus FLAG tag were as follows.

Wild-type TF:

Forward primer

TATATTGC GGC CGCCATGGAGACCCCTGCCTGGCCC

Reverse and complementary primer for cloning

TCGCCGGGATCCTCACTTGTCATCGTCATCCTTGTAATCCATTGAAACATTCAGTGG

TFdelC (1-274 amino acids of TF)

Reverse complementary primer

CCGCCGGGATCCTCACTTGTCATCGTCATCCTTGTAATCCATGTGTAGAGATATAGCCAG

Viral particles and generation of stable cell lines: Retroviral constructs with FLAG-tagged wild type TF and TFdelC were co-transfected in HEK293T packaging cells along with packaging pG, envelope, and Rev vectors pGP using Lipofectamine 2000 per manufacturer instructions. Medium containing active viral particles collected after 48 hours was centrifuged and stored at -80° C. For viral transduction, the cells were seeded at 50-60% confluence. The target cells were treated overnight with medium containing active viral particles along with hexadimethrine bromide (Sigma), a cationic polymer, to increase the efficiency of infection. Puromycin (Sigma) selection was initiated after 24 hours. The cells were harvested after 4 days to examine the effect on protein concentrations.

TF stability assay, ubiquitination assay: vSMCs and HEK293T were treated with 80 μM cycloheximide at different time intervals and were harvested for the stability assay. The ubiquitination of TF was examined by pretreating vSMCs and STUB1 KO and WT mice with the proteasome inhibitor MG132 (Boston Biochem) at 10 μM for 4-18 hours followed by immunoprecipitation as described above. vSMCs cell lysates were treated with uremic serum or solutes for 24 hours using 50 mM Tris buffered saline (pH 8.0) with 1% Triton X-100 and

centrifuged at 14,000 g for 20 minutes. The eluent were resolved on SDS-PAGE gel and probed with anti-ubiquitin antibody.

Immunostaining: Paraffin-embedded tissue blocks of de-identified patients were used after approval from the Institutional Review Board of Boston University Medical Center for immunofluorescence studies. Briefly, tissue blocks were sectioned at 4 μm and subjected to heat-induced antigen retrieval using 10 mM sodium citrate, pH 6.0. Normal goat serum (10%) and 1% BSA in 1X PBS/0.3% Triton X-100 were used as blocking agents. Tissue sections were incubated with STUB1 (Santa Cruz) and TF (Abcam) overnight at 4°C. Tissue sections were then washed and incubated with Alexa Fluor 488 or 594 conjugated secondary antibodies at room temperature for 1 hour. DAPI (Invitrogen) was used for the staining of nuclei, and then slides were mounted with fluorescence mounting medium (Dako). Images were obtained with the LeicaSP5, a point-scan epifluorescence laser confocal microscope.

Synthesis of recombinant STUB1 and in vitro binding assay: GST purification was performed as previously described *(29)*. Briefly, BL21 chemically competent *E. coli* (Invitrogen) were transformed with pGEX-2T STUB1 or pGEX-constructs obtained from Dr. Cam Patterson (University of North Carolina, Chapel Hill). Protein expression was induced in early log phase (OD_{600} of 0.6-0.8) by isopropyl-beta-D-thiogalactopyranoside (IPTG) (Invitrogen). Bacteria were lysed with lysozyme (American Bioanalytical) and 1% Triton X-100, followed by brief sonication. GST-tagged proteins were purified by passing the bacterial lysates over a glutathione sepharose 4B bead slurry (GE Healthcare). Purified GST-STUB1 protein was used in an in vitro binding assay with 1500 pM recombinant tissue factor Recombinant lipidated TF protein was obtained from Hematological Technologies.

TF procoagulant activity: TF surface/procoagulant activity was measured using a two-step FXa generation assay. A standard curve was generated by incubating human, recombinant lipidated TF (Enzolifesciences, Cat# SE-537) ranging from 0-500 pM along with 5 nM of human factor VIIa (Enzyme Research Laboratories Cat# HFVIIa), 150 nM of factor X (Enzyme

Research Laboratories Cat# HFX 1010), and 5 mM $CaCl_2$ for 30 minutes at 37^0C. The reaction mixture was incubated with chromogenic substrate for factor Xa (Chromogenix Cat# S2765, 1 mM final concentration). The reaction was stopped after 5 minutes using 10 μl of 50% glacial acetic acid and read at 405 nm absorbance. The TF procoagulant activity was examined in 96-well plate format with 5000 vSMCs or STUB1 KO and WT cells seeded per well. The cells were serum-starved for 16 hours and treated with IS or 5% pooled uremic serum with or without CH223191 or YL-109 for 24 hours. Cells were washed with TBS (50 mM Tris HCl, 120 mM NaCl, 2.7 mM KCl, 3 mg/ml BSA, pH=7.4) and incubated with 55 μl TBS containing 5 nM of human factor VIIa, 150 nM of factor X, and 5mM $CaCl_2$ for 30 minutes at 37^0C. 50 μl of the supernatant was incubated with chromogenic substrate at 1 mM final concentration. The reaction was stopped after 5 minutes by adding 10 μl of 50% glacial acetic acid, and the absorbance was read at 405 nm. TF activity for samples was calculated using linear regression analysis and normalized to the number of cells. The numbers of cells were determined using an MTT assay. The amount of compound needed to inhibit TF activity by 50% was considered to be the IC_{50} for the compound.

MTT assay: The numbers of cells were determined using alamarBlue assay reagent from Thermo Fisher Scientific. AlamarBlue cell viability reagent was used to measure the number of cells. To create the standard curve, serial dilution of VSMCs cells was performed in a black, clear-bottom 96-well plate. Cells were treated with alamarBlue for one hour. After one hour, the fluorescence intensity of alamarBlue was measured at 570 nm using an infinite microplate reader from Tecan. As described in the reagent protocol from Thermo Fisher, the fluorescence readout using alamarBlue was linear over the range from ~500 to 50,000 cells. By serial dilution of cells, we obtained a linear standard curve with $R^2 = 0.97$, which was applied for counting the cells. For TF normalization, after the TF activity measurement, cells were washed with 1X PBS, and then 100 μl of medium was added and incubated with alamarBlue for one hour at 37 ºC in

an incubator supplied with 5% CO_2 in the cell incubator. The fluorescence was measured at 750 nm, and the standard curve was applied to count the number of viable cells. The amount of compound needed to inhibit TF activity by 50% was considered as the IC50 for the compound.

Correlation of changes in TF expression and thrombogenicity in mice exposed to YL1-09 and IS: We correlated the reduction of TF in the aortic lysates of individual mice exposed to YL-109 with the prolongation of TtO, with the hypothesis that these parameters might inversely correlate. We analyzed seven mice from two groups: IS and IS + YL-109. First, we quantified the expression of TF in the aortic lysates of IS-treated animals using ImageJ and averaged them. GAPDH served as a loading control. This average TF expressions in the IS group were then used to estimate the changes in TF in the aortae of YL-109 + IS animals:

change in TF expression in an individual YL-109 treated animal = (amount of TF in YL-109 + IS)/(average TF in IS animals)

A similar approach was used to determine the changes in TtO in individual animals in YL-109 + IS group:

change in TtO in an individual YL-109 treated animal = (TtO in YL-109 + IS)/(average TtO in IS animals)

Spearman's rank correlation analysis was used to correlate the TtO and TF concentrations in individual mice in the IS + YL-109 group.

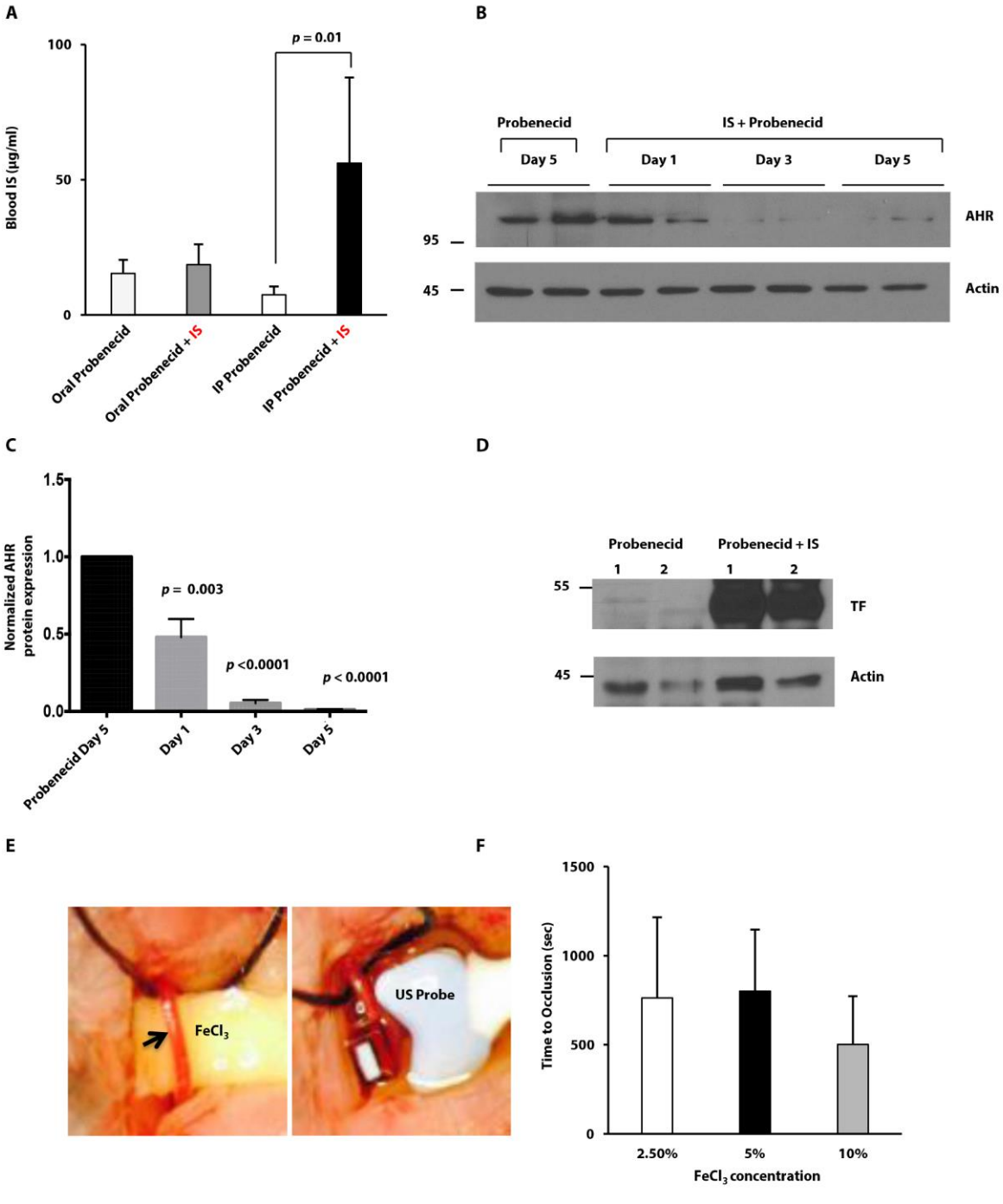
A
Blood IS (µg/ml)
100
50
0
p = 0.01
Oral Probenecid
Oral Probenecid + IS
IP Probenecid
IP Probenecid + IS
B
Probenecid
IS + Probenecid
Day 5
Day 1
Day 3
Day 5
95
45
AHR
Actin
C
Normalized AHR protein expression
1.5
1.0
0.5
0.0
p = 0.003
p <0.0001
p < 0.0001
Probenecid Day 5
Day 1
Day 3
Day 5
D
Probenecid
Probenecid + IS
1
2
1
2
55
45
TF
Actin
E
FeCl3
US Probe
F
Time to Occlusion (sec)
1500
1000
500
0
2.50%
5%
10%
FeCl3 concentration

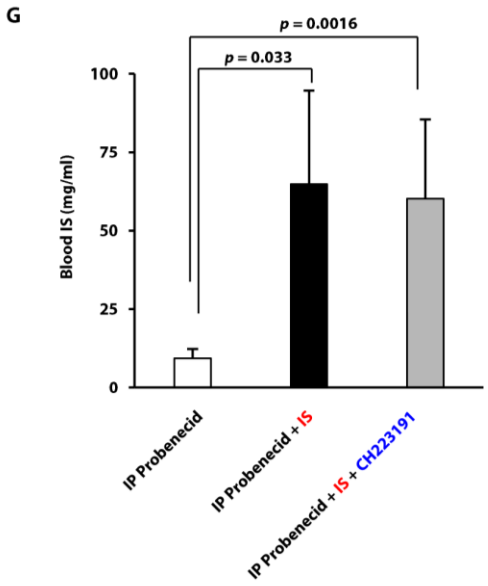

Supplementary figure 1. An indolic solute–specific animal model.

(A) Selection of IS protocol that increases blood concentration of IS similar to ESRD patients. For this experiment and other animal experiments described in the supplementary materials, groups of 10- to 14-week-old C57BL/6 male and female mice were used. Different protocols consisting of IS administration in drinking water (4 mg/ml) along with probenecid (150 mg/kg) given twice a day by intraperitoneal injection were tested in five mice per group. The blood samples were collected at the end of 5 days, and the average IS concentrations for different groups are shown. Data shown as means ± SD. The group receiving 4 mg/ml IS dissolved in drinking water and 150 mg/kg probenecid intraperitoneally twice daily yielded consistently high IS concentrations above 40-50 µg/ml, which are similar to patients with CKD stage 5/ESRD *(11)*. As a result, this protocol was chosen for subsequent experiments. No significant differences in IS concentrations were observed between male and female mice.

(**B**) Degradation of AHR protein in the aortae of mice exposed to IS + probenecid. C57BL/6 12- to 14-week-old male and female mice were given probenecid 150 mg/kg IP twice a day with or without IS 4 mg/ml in water for 5 days (n = 4 animals per group). The aortae harvested at the indicated time point were lysed and probed for AHR, with actin serving as a loading control. The

AHR band was normalized to the intensity of the actin band using ImageJ. A representative blot from two out of four animals per time point is shown.

(**C**) Persistent AHR activation within the vessel walls of mice exposed to IS + probenecid. Averages of normalized AHR expression in the aortic lysates of four mice at the indicated times are shown. Data shown as means ± SD. p values compare each group to the probenecid control group harvested at day 5.

(**D**) Increase in TF in the aortae of IS-injected animals. The C57BL/6 animals exposed to IS and probenecid were euthanized, and the thoracic and abdominal aortae were harvested, lysed in RIPA buffer, and sonicated. The lysates were probed for TF and actin. Lysates of two animals from five mice per group are shown.

(**E**) Induction and measurement of thrombogenicity using the carotid artery thrombosis model. The carotid artery (shown by a black arrow) was exposed in the anesthetized animals, and thrombosis was induced using a 10% strip of $FeCL_3$ placed below the carotid artery for one minute, after which an ultrasound probe ("US Probe") was used to measure the blood flow.

(**F**) Selection of concentration of $FeCl_3$ that consistently resulted in thrombosis in the uremic milieu. With the above protocol (IS and probenecid), we examined different concentrations of $FeCl_3$ strips (2.5%-10%) applied below the carotid artery, and the blood flow was monitored for 20 minutes. The time for the flow to drop to 0-0.299 ml/min was considered as the Time to occlusion (TtO). An average of four animals is shown in each group. 10% $FeCl_3$ resulted in smallest standard deviation and was adopted for subsequent experiments. Data shown as means ± SD. **(G**) Blood concentrations of IS in mice exposed to IS or IS + CH223191 compared to the control animals. An average of IS concentrations from five animals measured at the end of 5 days is shown. Student's t-test was performed. Data shown as means ± SD.

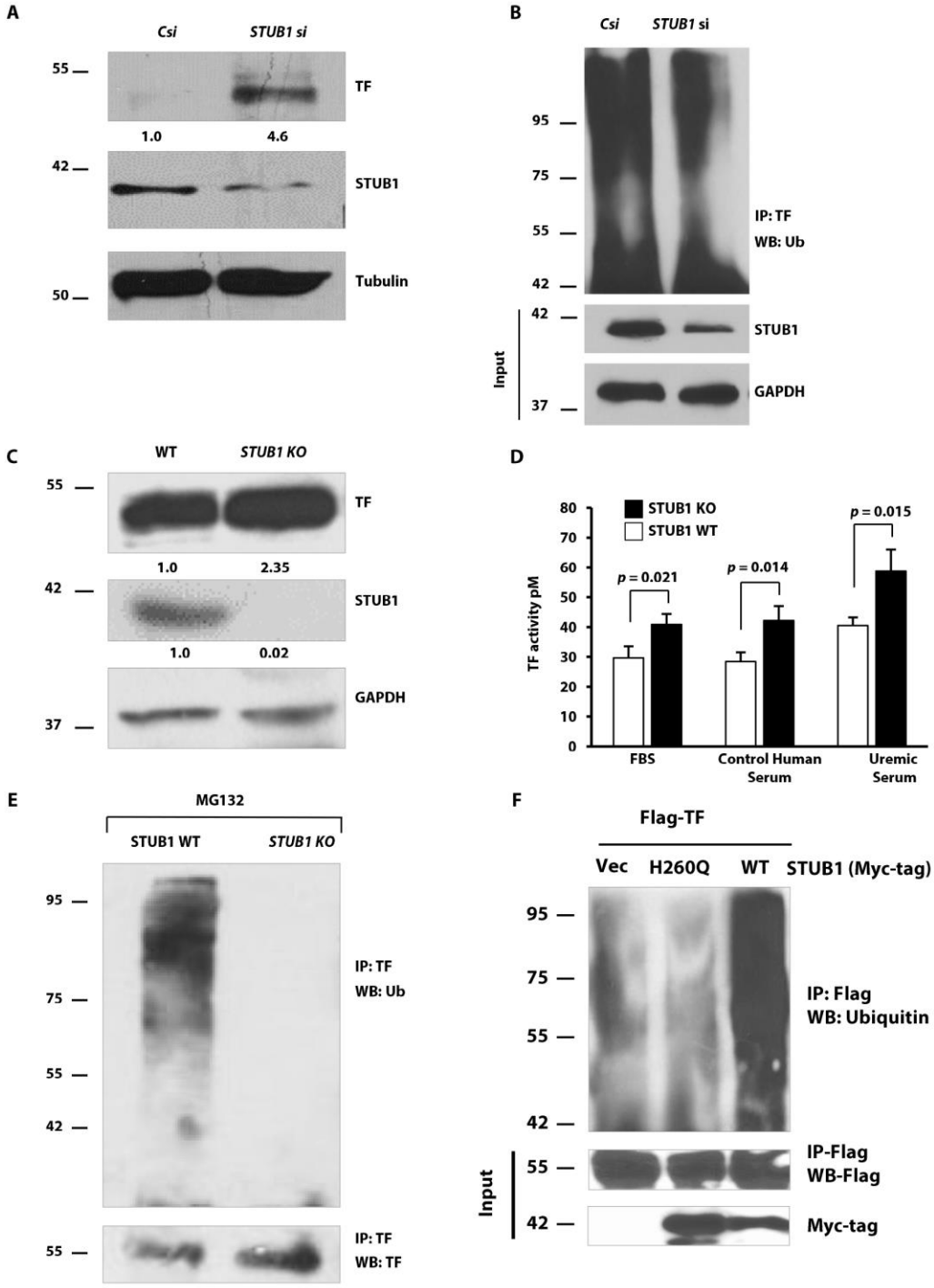

Supplementary figure 2. **STUB1 regulation of TF protein.**

(**A**) Immortalized human umbilical vein endothelial cells (HUVEC-Tert) seeded in 6-well plates were transiently transfected with STUB1 (*STUB1si*) and control siRNA oligos (*Csi*). The cells were lysed after 48 hours and probed for TF and tubulin. Equal amounts of lysates were

separately probed for STUB1. A representative blot from two independent experiments performed in duplicate is shown. A significantly higher (more than four-fold) TF expression was noted with *STUB1* silencing ($p = 0.001$).

(**B**) vSMCs pretransfected with control (*Csi*) or *STUB1* (*STUB1s*i) siRNA oligos treated with 10 μM MG132 for 4 hours were lysed and immunoprecipitated with TF antibody, then probed using anti-ubiquitin (Ub) antibody. The lysates were probed for STUB1 and GAPDH to confirm STUB1 silencing. A representative blot of two independent experiments performed in duplicate is shown.

(**C**) Mesenchymal embryonic fibroblasts (MEFs) from STUB1 KO and WT animals seeded for 48 hours were lysed and probed for TF and GAPDH, where the latter served as a loading control. Equal amounts of lysates were separately probed for STUB1. The values below the blot represent the TF bands normalized against the loading control using ImageJ. A representative of four independent experiments is shown. $p = 0.003$ for the difference in TF between STUB1 KO and WT MEFs.

(**D**) *STUB1* KO and WT MEFs serum-starved overnight were stimulated with 5% uremic serum (pooled from twenty patients with ESRD (uremic serum) *(8),* non-uremic control human serum (age-, gender-, and ethnic background-matched healthy controls), or fetal bovine serum (FBS), and subjected to TF activity assay after 24 hours. An average of two independent experiments performed in duplicate is shown. In STUB1 WT cells, TF activity significantly increased with uremic serum compared to control serum ($p = 0.006$). The p values in the figure are for the comparison of TF activity in STUB1 KO and STUB1 WT cells in each group. Student's t-test was performed. Data shown as means ± SD.

(**E**) STUB1 WT and KO MEFs treated with 10 μM MG132 for 4 hours were lysed and immunoprecipitated with TF antibody and then probed using anti-ubiquitin antibody (Ub). The blot was stripped and reprobed using TF antibody for the immunoprecipitated TF. A representative blot of two independent experiments performed in duplicate is shown.

(**F**) HEK293T cells were cotransfected with FLAG-tagged TF and MYC-tagged wild-type STUB1 (WT) or the U-box mutant H260Q STUB1 (H260Q). The cells were treated with MG132 (10 μM), and the lysates were prepared in RIPA buffer, immunoprecipitated with TF antibody, and probed with ubiquitin antibody. The blot was stripped and reprobed with TF to compare the immunoprecipitated TF in all three groups. Five percent of lysates were probed with anti-MYC antibody. A representative from two separate experiments performed in duplicate is shown.

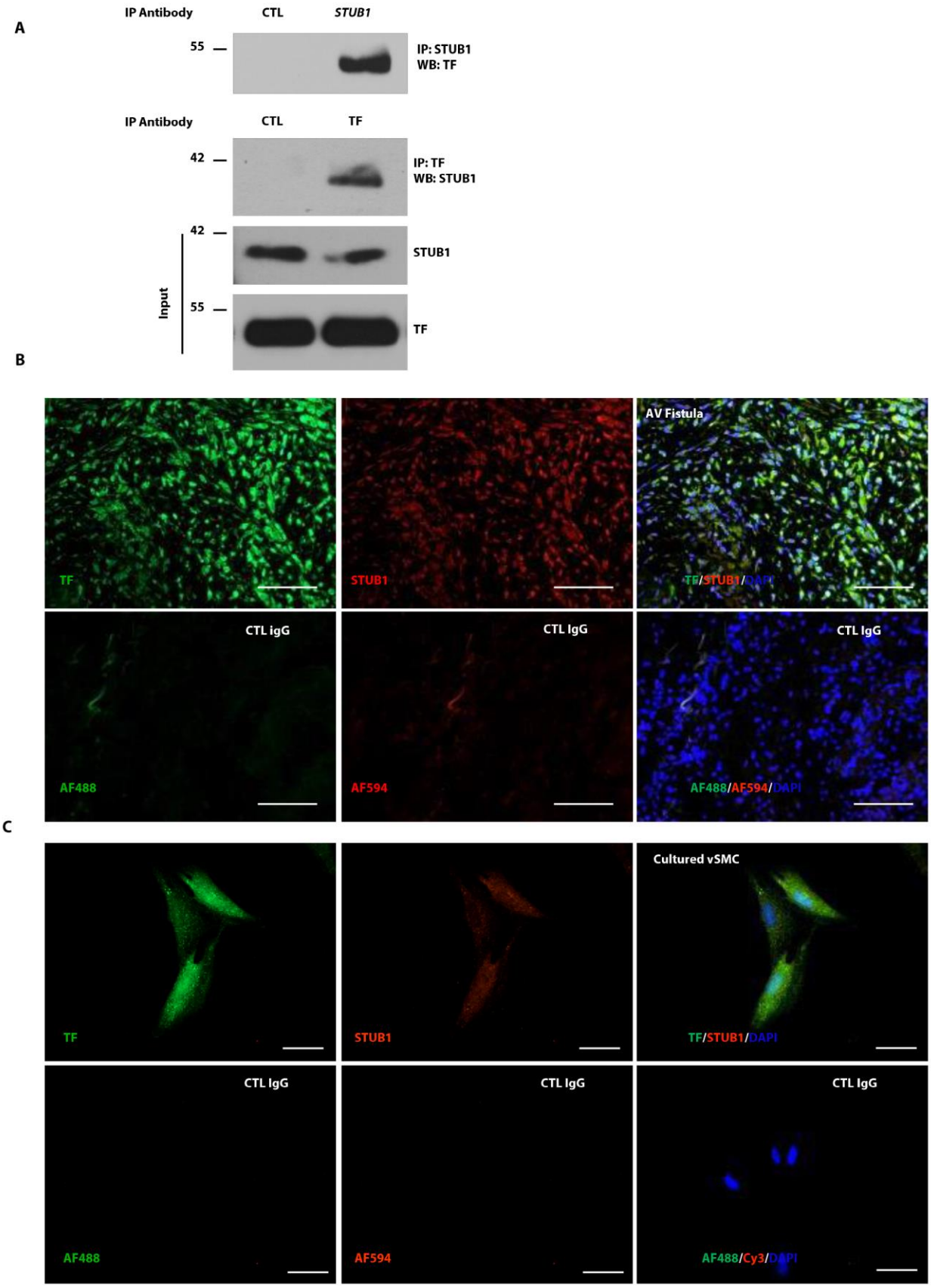
A
IP Antibody
CTL
STUB1
55
IP: STUB1
WB: TF
IP Antibody
CTL
TF
42
IP: TF
WB: STUB1
42
STUB1
Input
55
TF
B
TF
STUB1
AV Fistula
TF/STUB1/DAPI
CTL IgG
CTL IgG
CTL IgG
AF488
AF594
AF488/AF594/DAPI
C
TF
STUB1
Cultured vSMC
TF/STUB1/DAPI
CTL IgG
CTL IgG
CTL IgG
AF488
AF594
AF488/Cy3/DAPI

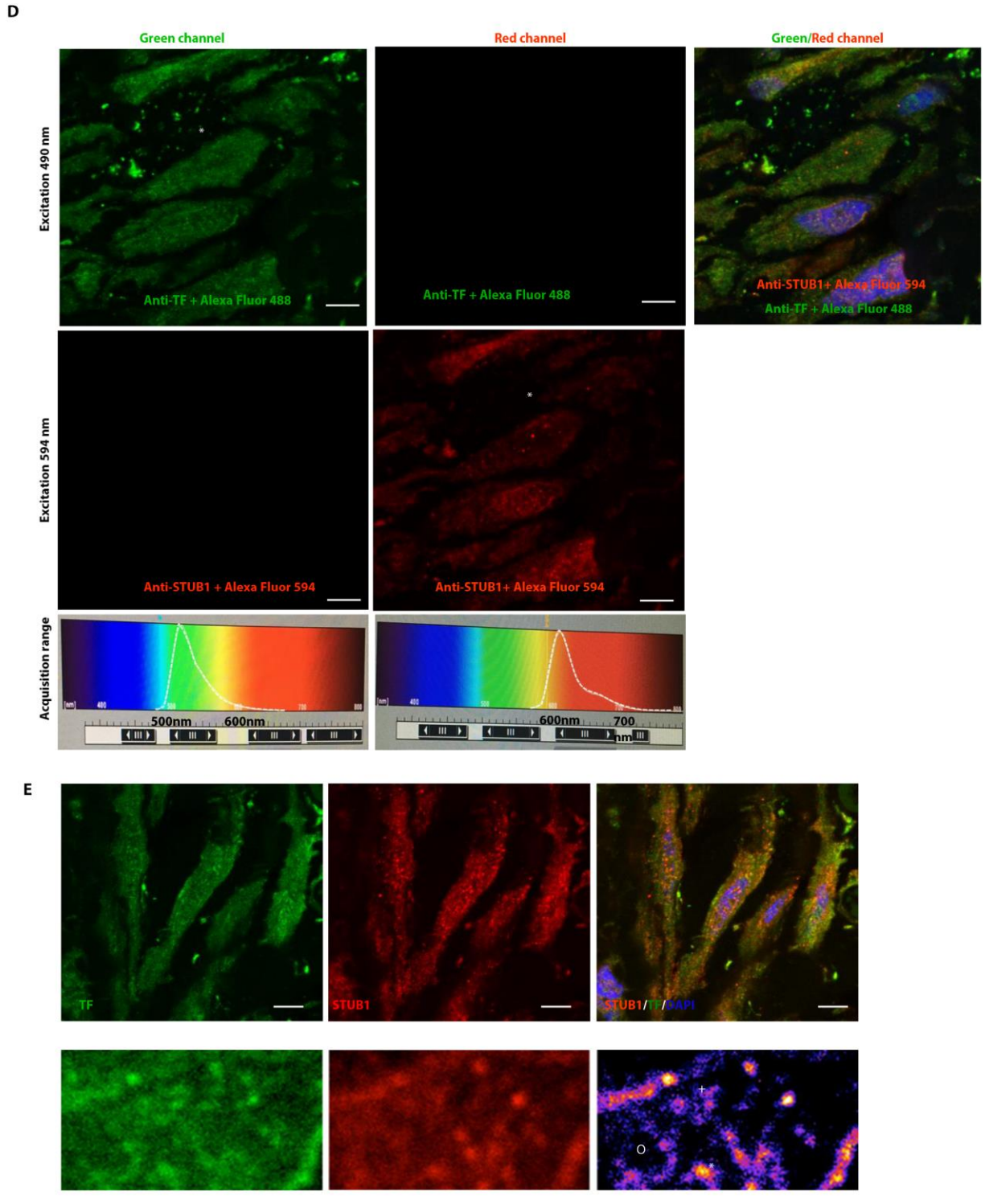
D
Green channel
Red channel
Green/Red channel
Excitation 490 nm
Anti-TF + Alexa Fluor 488
Anti-TF + Alexa Fluor 488
Anti-STUB1+ Alexa Fluor 594
Anti-TF + Alexa Fluor 488
Excitation 594 nm
Anti-STUB1 + Alexa Fluor 594
Anti-STUB1+ Alexa Fluor 594
Acquisition range
500nm
600nm
600nm
700
nm
E
TF
STUB1
STUB1/TF/DAPI

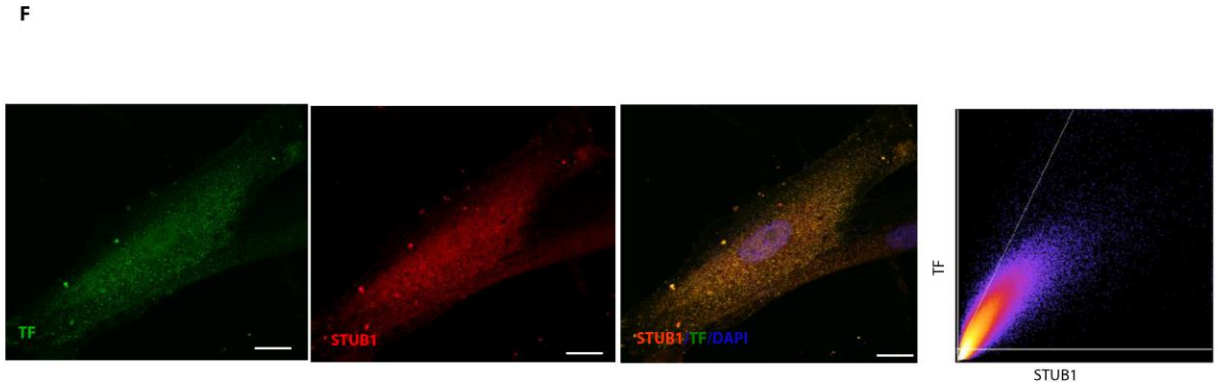

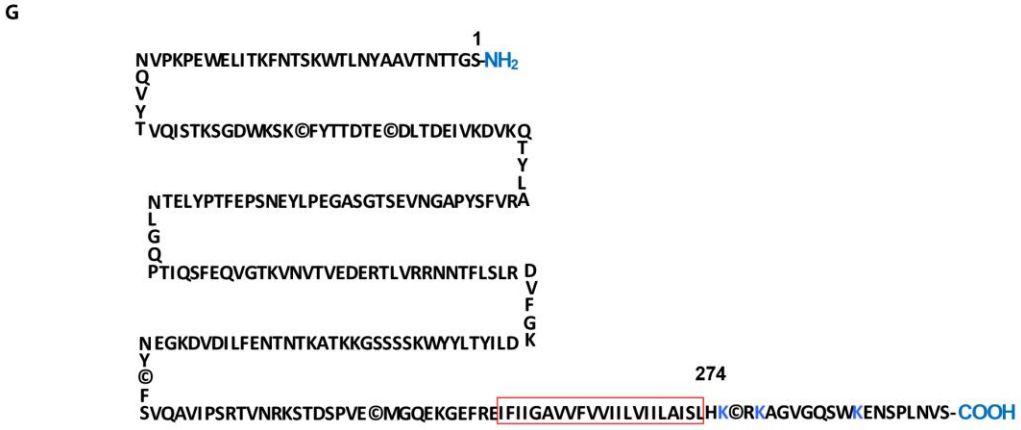

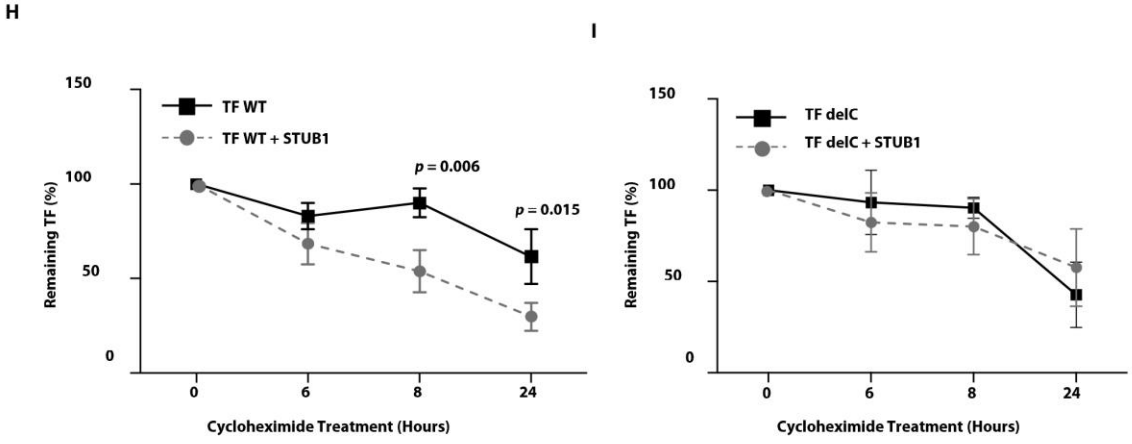

Supplementary figure 3. STUB1 interaction with TF.

(**A**) Primary human aortic vMSCs were lysed and subjected to immunoprecipitation with anti-TF (TFH10) antibodies and eluents were probed for STUB1 and vice versa. The blots were stripped and reprobed for TF or STUB1 to compare the immunoprecipitated proteins. Isotype antibodies

served as controls (CTL). Five percent of whole cell lysates are shown as inputs. A representative from two independent experiments performed in duplicate is shown.

(**B**) An AVF explant from a 42-year-old Hispanic male (Patient # 2 in table S1) was paraffin-embedded and stained with anti-TF anti-mouse and anti-STUB1 anti-rabbit antibodies and isotype-matched control antibodies (CTL IgG, Thermo Fisher Scientific) at the same dilutions. DAPI was used to stain the nuclei. Representative images from ten random areas are shown. Scale bar = 100 μM.

(**C**) Early passage (passage 4) primary vascular smooth muscle cells were fixed and stained with the same antibodies as in (B) and were examined using a confocal microscope. Scale bar = 10 μM.

(**D**) Paraffin-embedded sections of an explanted AVF from a 47-year-old male patient (# 3 from table S1) were stained with anti-TF and anti-STUB1 antibodies and secondary antibodies conjugated with AF488 and AF594 fluorophores. Each fluorophore was excited with the appropriate laser, and the signal was acquired in both the red and green channels to test for any bleed-through. Several images were acquired at the same microscope settings such as gain and exposure time using a Leica SP5 confocal microscope, and the representative images are shown. Scale bar = 10 μM. The lower panels show the ranges of acquisition of signal in both channels. The asterisk marks a cell with lower STUB1 and higher TF expression, as seen in Fig. 3G.

(**E**) (Upper panel). The paraffin-embedded section of normal temporal artery from a 63-year-old female *(11)* was stained with anti-TF and anti-STUB1 antibodies and secondary antibodies conjugated with 488 and 594 fluorophores, respectively. The slides were examined using a confocal microscope Leica SP5 with an argon laser, and the collected images were analyzed using ImageJ. The merged image for three channels is shown in the last panel. Scale bar = 10 μM. (Lower panel) The colocalization was mathematically derived using an approach that was previously described *(27)*. In this method, the colocalization between two proteins takes into

consideration normalized covariance or the correlation coefficient between 2 sets of data. A montage image created in ImageJ using a 1.791x3.21 μm area within vSMCs from the upper panel. STUB1 (red) and TF (green) appear as their labeled fluorophores, and the last panel shows the colocalization areas mathematically derived with the equation described by Kriber *et al (27)* and displayed as an artificial color (FIRE from ImageJ). A white cross marks a representative area of colocalization between STUB1 and TF. The highest amounts of colocalization appear as distinct areas of punctate yellow staining (marked by an asterisk), and absence of colocalization is displayed as black area (marked by an open circle). A Pearson's correlation coefficient of 0.50 was obtained, which supports the colocalization of STUB1 and TF in vSMCs of a normal human artery *(27)*.

(**F**) Early passage primary human aortic vSMCs were fixed and subjected to immunofluorescence protocols using anti-TF and anti-STUB1 antibodies. DAPI was used to stain nuclei. The cells were imaged using confocal Leica500 microscope. One representative cell among fifty randomly selected cells is shown. ImageJ program was used to analyze colocalization, which was displayed as a scatter plot, where the relative pixel intensities for both proteins were plotted on two axes, and the colocalization was shown on the Z-axis *(11)*. The correlation analysis performed on the distribution of pixel intensities using ImageJ showed a Pearson's correlation coefficient of 0.82, supporting colocalization between TF and STUB1 in unstimulated vSMCs.

(**G**) A schematic of TF protein is shown with an extracellular N-terminus, a small intramembranous domain (marked by a red box), and an intracytosolic C-terminus tail, which harbors several lysine residues (highlighted as blue "K"), which can be putative sites for polyubiquitination. The C-terminus deletion of TF (TF delC) contains 1-274 amino acids. The 'N' represents putative N-linked glycosylation sites and five half-cystine residues are represented as © (*29*).

(**H**) Densitometry was performed on TF expression in Fig. 3D with ImageJ, using GAPDH to normalize the TF expression, which was represented as a percentage of TF at time 0. The time to reach 50% of initial TF is considered as the TF half-life. An average TF expression from four experiments is shown at each time point. Data shown as means ± SD. (**I**) Densitometry was performed on TF expression in Fig. 3E using ImageJ as above. An average TF from four experiments is shown at each time point. Data shown as means ± SD.

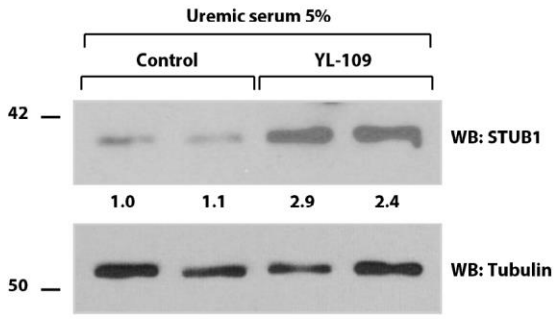

Supplementary figure 4. STUB1 expression in the YL-109–treated flow loops. vSMCs lining the flow loops treated with IS (10 μM) with or without YL-109 (25 μM) were lysed in RIPA buffer and probed for STUB1. Two representative samples out of six flow loops are shown.

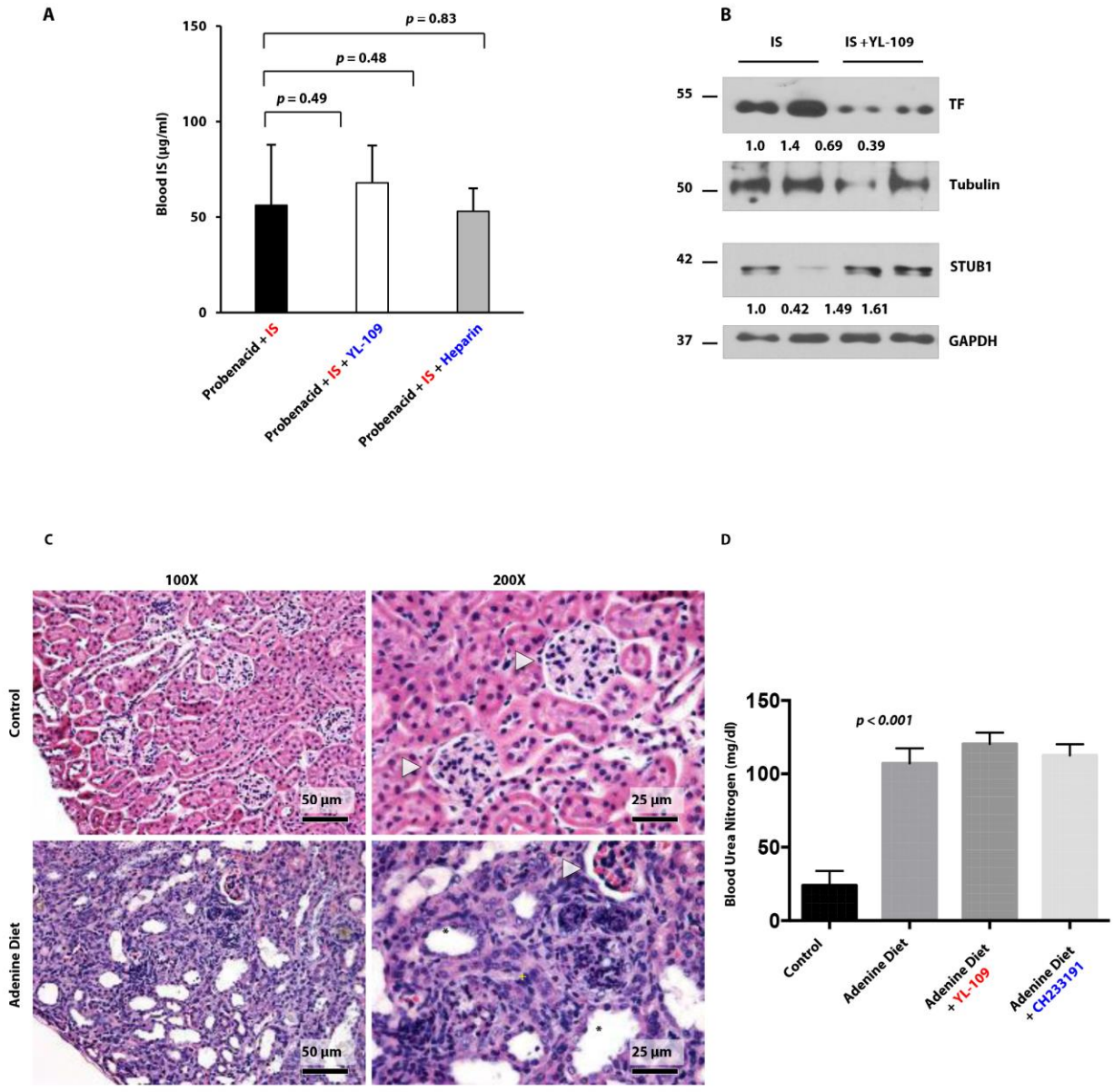

Supplementary figure 5. AHR or STUB1 manipulation in uremic animal model.

(**A**) Average IS concentrations from mice before the thrombosis assay in Fig. 5C are shown. Data shown as means ± SD. **(B)** YL-109 increases STUB1 and reduces TF expression in the aortae of the uremic animals. The C57BL/6 animals exposed to IS (4 mg/ml) in water and probenecid (150 mg/kg) IP with or without YL-109 (5 mg/kg) for 5 days were euthanized, and the thoracic and abdominal aortae were harvested and lysed in RIPA buffer and sonicated. TF

and STUB1 expression was normalized to tubulin and GAPDH, respectively. Representative blots of two mice from groups of five are shown.

(**C**) Adenine-induced CKD model shows chronic tubulointerstitial injury. Kidneys harvested from 10- to 14–week-old C57BL/6 male and female mice exposed to a diet containing 0.25% adenine for two weeks were embedded in paraffin and stained with hematoxylin & eosin. Compared to the animals on regular chow, the adenine-treated animals showed evidence of glomerular loss (white arrowhead), reduction in the tubular mass (black asterisk), presence of inflammatory infiltrate, and tubulointerstitial fibrosis (yellow cross). Scale bar = 50 μM and 25 μM for 100X and 200X magnification images, respectively.

(**D**) Increase in BUN in adenine CKD model. Plasma samples obtained at the end of two weeks were analyzed. An average BUN value of five mice per group is shown. Data shown as means ± SD. The adenine-treated animals showed 5-fold increase in BUN compared to the control group on normal chow ($p < 0.001$), and these values corresponded to those detected in patients with advanced CKD *(11)*. Compared to the adenine-treated group, there were no differences in BUN values in animals exposed to YL-109 or CH223191.

Supplementary Table 1. Demographic and clinical characteristics of patients included in the study to examine the vascular expression of STUB1 and TF.

No	Age	Ethnicity	Gender	Cause of ESRD	Cause for AVF removal	eGFR	DM	HT	BMI	Hb	Platelets	INR	SBP	DBP
	Uremic													
1	35	Hispanic	Male	HTN	Aneurysmal, thrombotic, and painful AVF	18	0	1	29	14.2	160	1.03	159	80
2	42	Hispanic	Male	DM, HTN	Superficial ulceration of skin overlying left radiocephalic AVF, aneurysm	<5	1	1	47.8	12.2	217	0.95	119	67
3	47	Hispanic	Male	HTN	Venous hypertension secondary to AVF and proximal obstruction	<5	0	1	39.5	12.2	234	0.9	107	55
4	70	Black	Female	HTN, DM	Ulceration over AVF	<5	1	1	42	11.2	203	1.37	134	76
	Non-uremic control*													
	Age	**Ethnicity**	**Gender**	**Cause of amputation**		**eGFR**	**DM**	**HT**	**BMI**	**Hb**	**Platelets**	**INR**	**SBP**	**DBP**
1	66	Hispanic	Male	Malignant tumor		>90	1	1	23	10.7	180	1.13	169	77
2	64	Caucasian	Female	Malignant tumor		>90	0	0	31.3	9	433	1.08	117	71
3	49	Black	Male	Non healing ulcer		>90	1	0	27	11	318	1.0	105	82
4	53	Hispanic	Male	Malignant tumor		>90	0	0	30	11.8	118	0.9	110	81

eGFR= estimated GFR ml/min/1.73 m^2
DM = diabetes (1 = present, 0 = absent)
HT= hypertension (1 = present, 0 = absent)
BMI = body mass index
Hb = hemoglobin (gm/dl)
Platelets = 1000/1 µl blood
INR = international normalized ratio
SBP = systolic blood pressure (mm Hg)
DBP = diastolic blood pressure (mm Hg)
* = tissue taken from the most distant site from the lesion